JGR Solid Earth

RESEARCH ARTICLE
10.1029/2024JB029213

Decoding Stress Patterns of the 2023 Türkiye-Syria Earthquake Doublet

Jianquan Chen[1], Chang Liu[1], Luca Dal Zilio[2,3], Jianling Cao[4], Hui Wang[4], Guangliang Yang[5], Oğuz H. Göğüş[6], Hang Zhang[1], and Yaolin Shi[7]

[1]State Key Laboratory of Marine Geology, Tongji University, Shanghai, China, [2]Earth Observatory of Singapore, Nanyang Technological University, Nanyang Ave, Singapore, [3]Asian School of the Environment, Nanyang Technological University, Nanyang Ave, Singapore, [4]Institute of Earthquake Forecasting, China Earthquake Administration, Beijing, China, [5]Institute of Seismology, China Earthquake Administration, Wuhan, China, [6]Istanbul Teknik Üniversitesi, Avrasya Yer Bilimleri Enstitüsü, Ayazaga, Istanbul, Türkiye, [7]Key Laboratory of Computational Geodynamics, Chinese Academy of Sciences, Beijing, China

Key Points:

- The 2023 Mw 7.8 earthquake was delayed due to stress shadow caused by historical earthquakes between 1822 and 2023
- The 2023 Mw 7.6 earthquake was promoted caused by historical earthquakes and finally triggered by the 2023 Mw 7.8 earthquake
- Special attention should be paid to the raised seismic hazards in the seismic gap of the northeastern EAF and the northern DSF

Supporting Information:

Supporting Information may be found in the online version of this article.

Correspondence to:

C. Liu,
changliuu@tongji.edu.cn;
changliuu@gmail.com

Citation:

Chen, J., Liu, C., Dal Zilio, L., Cao, J., Wang, H., Yang, G., et al. (2024). Decoding stress patterns of the 2023 Türkiye-Syria earthquake doublet. *Journal of Geophysical Research: Solid Earth*, *129*, e2024JB029213. https://doi.org/10.1029/2024JB029213

Received 31 MAR 2024
Accepted 14 OCT 2024

Author Contributions:

Conceptualization: Chang Liu
Data curation: Jianquan Chen, Chang Liu, Hang Zhang
Formal analysis: Chang Liu, Luca Dal Zilio, Yaolin Shi
Funding acquisition: Chang Liu, Luca Dal Zilio, Jianling Cao, Hui Wang, Guangliang Yang, Yaolin Shi
Investigation: Jianquan Chen, Chang Liu, Guangliang Yang, Oğuz H. Göğüş, Yaolin Shi
Methodology: Chang Liu
Project administration: Chang Liu
Resources: Chang Liu, Hui Wang
Supervision: Chang Liu
Validation: Jianquan Chen, Chang Liu, Luca Dal Zilio, Jianling Cao, Hui Wang, Guangliang Yang, Oğuz H. Göğüş, Hang Zhang, Yaolin Shi
Visualization: Jianquan Chen

Abstract Earthquake interaction across multiple time scales can reveal complex stress evolution and rupture patterns. Here, we investigate the role of static stress change in the 2023 Mw 7.8 and 7.6 earthquake doublet along the East Anatolian Fault (EAF), using simulations of 19 historical earthquakes (M ≥ 6.1) and the 2023 earthquake doublet from 1822 to 2023. Focusing on six cascading sub-events during the 2023 Kahramanmaraş earthquake doublet, we reveal how one sub-event's stress alteration can impact the emergence and rupture of subsequent sub-events. Our analysis unveils that the 2023 Mw 7.8 earthquake was delayed due to stress shadow effects from historical events, while the 2023 Mw 7.6 earthquake was accelerated as a result of stress increases from historical events and ultimately triggered by the 2023 Mw 7.8 earthquake. This study underscores the importance of grasping earthquake preparation, rupture initiation, propagation, and termination in the context of intricate fault systems worldwide. Based on these results, we draw attention to increased seismic hazards in the Elazig-Bingol seismic gap of the EAF and the northern section of the Dead Sea Fault (DSF), necessitating increased monitoring and preparedness efforts.

Plain Language Summary On 6 February 2023, a doublet of earthquakes (Mw 7.8 and 7.6) struck the borders between southeastern Turkey and northern Syria. Aiming to discover the influence of past earthquakes on the initiation, propagation, and termination of the doublet, as well as the prospective seismic hazards of the seismic gaps in the targeted region, we demonstrated spatiotemporal variations in stress along the EAF before, during, and after 2023 using the earthquake data during the past two centuries. We revealed how the stress changes induced by one sub-event can influence the occurrence and behavior of subsequent sub-events, and consequently on how the rupture process evolves over time and space. Our research is crucial for gaining insights into underlying mechanisms governing earthquake preparation, rupturing and propagation in earthquake sequences, and migration within the EAF. We also suggest special attention should be paid to the raised seismic hazards between the Palu and Ilica cities in the Elazig-Bingol seismic gap of the EAF and the northern section of the DSF due to stress loading. This might be helpful in the development of effective strategies for disaster prevention and relief in the regions of southeastern Turkey, northern Syria, and Lebanon.

1. Introduction

On 6 February 2023, a devastating earthquake doublet (Mw 7.8 and Mw 7.6) shook southeastern Türkiye and northern Syria (U.S. Geological Survey [USGS] Earthquake Hazards Program, 2017; see Data and Resources), causing widespread damage, homelessness, and over fifty thousand fatalities (Dal Zilio & Ampuero, 2023). The first earthquake, with a magnitude of Mw 7.8, occurred along the East Anatolian Fault (EAF) at coordinates 37.226°N, 37.014°E. The second, a Mw 7.6 event, took place on the Cardak Fault (CF), located at 38.011°N, 37.196°E, a splay fault linked to the EAF's Erkenek segment (Duman & Emre, 2013) (Figure 1). Both shallow-depth main shocks (10–14.5 km) generated intense ground motion, leading to catastrophic regional impacts (Dal Zilio & Ampuero, 2023; USGS Earthquake Hazards Program, 2017).

Previous studies have investigated the fault slip and dynamics rupture processes of the Mw 7.8 and Mw 7.6 earthquakes using Global Navigation Satellite System (GNSS), synthetic aperture radar (SAR), strong motion (SM), and seismic data (Barbot et al., 2023; K. Chen et al., 2024; Delouis et al., 2023; Gabriel et al., 2023;

Writing – original draft: Jianquan Chen, Chang Liu
Writing – review & editing: Chang Liu, Luca Dal Zilio, Jianling Cao

Goldberg et al., 2023; He et al., 2023; Jia et al., 2023; Li et al., 2023; Liu et al., 2023; Mai et al., 2023; Melgar et al., 2023; Okuwaki et al., 2023; Ren et al., 2024; USGS Earthquake Hazards Program, 2017; Wang et al., 2023; Xu et al., 2023; Zahradnik et al., 2023; Zhang et al., 2023). These studies suggest that each main shock involved three sub-events, rupturing three segments in the 2023 earthquake doublet (Tables S1 and S2 in Supporting Information S1). The rare occurrence of such large magnitude earthquake doublets with multiple sub-events within 9 hr warrants investigation into their interactions. Understanding how stress changes induced by preceding sub-events influence the occurrence and behavior of subsequent sub-events can provide insights into the rupture process's spatiotemporal evolution. However, limited research has explored the interactions between cascading sub-events in earthquake sequences or doublets.

Sunbul (2019) previously identified that the 2023 Mw 7.8 earthquake's Pazarcik segment of the EAF was stress-loaded by historical earthquakes before 2019. Notably, the 2020 Mw 6.7 Elazig earthquake, which occurred near the 2023 Mw 7.8 earthquake rupture's northeastern end (Güvercin et al., 2023; Okuwaki et al., 2023; USGS Earthquake Hazards Program, 2017), was absent from Sunbul's (2019) stress calculations (Figure 1). This raises questions about the Elazig earthquake's potential impact on the 2023 Mw 7.8 earthquake rupture process. Considering the Elazig earthquake's magnitude, proximity to the 2023 Mw 7.8 earthquake rupture, and exclusion from previous stress calculations, it's crucial to evaluate its stress change contribution along the EAF. Furthermore, the stress change on the CF caused by pre-2023 historical earthquakes and its influence on the 2023 Mw 7.6 earthquake remain unclear.

The EAF, a critical tectonic boundary separating the Arabian and Anatolian plates, spans approximately 580 km from its intersection with the North Anatolian Fault (NAF) in the northeast to its connection with the Dead Sea Fault (DSF) in the southwest (Arpat and Şaroğlu, 1972; Hempton et al., 1981; Jackson & McKenzie, 1984; Lyberis et al., 1982; Muehlberger & Gordon, 1987; Reilinger et al., 2006; Sunbul, 2019; Taymaz et al., 2021; Türkelli et al., 2003). Two seismic gaps, the Kahramanmaras-Malatya and Elazig-Bingol gaps, have been identified on the EAF based on seismic data from 1822 to 2019 (Güvercin et al., 2022; Nalbant et al., 2002; Sunbul, 2019). The 2023 Mw 7.8 earthquake filled the Kahramanmaras-Malatya gap (Mai et al., 2023; Melgar et al., 2023; Okuwaki et al., 2023; USGS Earthquake Hazards Program, 2017) (Figure 1).

Numerous large strike-slip earthquakes ($M \geq 6.1$) have occurred within and near the EAF over the past two centuries, as evidenced by the historical earthquake catalog (Table 1). A key question arises: how do stress perturbations resulting from these earthquakes influence seismic activity and hazards along the EAF? Another essential question is how the stress changes induced by past earthquakes affected the initiation, propagation, and termination of the 2023 earthquake doublet.

Nalbant et al. (2002) and Sunbul (2019) computed stress changes on different segments of the EAF induced by 18 historical earthquakes (Nos. 1–10, 14–21) predating 2019. Their work preliminarily identified two stress loaded seismic gaps: the Kahramanmaras-Malatya segment in the EAF, the Yedisu Segment in the NAF. Notably, their earthquake catalog did not include three significant events: the 2020 Mw 6.7 Elazig earthquake and the 2023 Mw 7.8 and 7.6 earthquake doublet. Their study also did not account for the stress changes on the CF, which was ruptured by the Mw 7.6 earthquake, nor its impact on each sub-event of the 2023 earthquake doublet. The stress change in the seismic gap Elazig-Bingol still remains unclear (Figure 1). Toda and Stein (2024) found that the Mw 7.6 earthquake was promoted by the Mw 7.8 earthquake by investigating the interactions of the three large earthquakes ($Mw \geq 6.8$) on the EAF since 2020. However, their earthquake catalog lacked 18 significant events in and around the EAF before 2020. Consequently, they missed the opportunity to investigate the stress changes on different segments of the EAF and CF caused by those 18 historical earthquakes, as well as the interaction processes between the six cascading sub-events during the 2023 earthquake doublet.

Here, we address these questions using simulations of the Coulomb Failure Stress (ΔCFS) before, during, and after the 2023 doublet induced by 21 earthquakes ($M \geq 6.1$), including the 2023 doublet, based on existing focal mechanisms in and around the EAF from 1822 to 2023. Our goal was to evaluate spatiotemporal stress variations along the EAF, elucidate the interactions between the six cascading sub-events of the 2023 doublet, and assess future seismic hazards in the region. Our research provides insights into earthquake rupture initiation, propagation, and termination within the EAF and other large-scale strike-slip fault zones. Moreover, our findings can inform disaster prevention and relief strategies in southeastern Türkiye, northern Syria, and Lebanon. In this paper, we first simulated and demonstrated the stress distribution along each sub-event of the 2023 earthquake doublet, considering the impacts of historical earthquakes from 1822 to 2023. We then analyzed the interaction

10.1029/2024JB029213

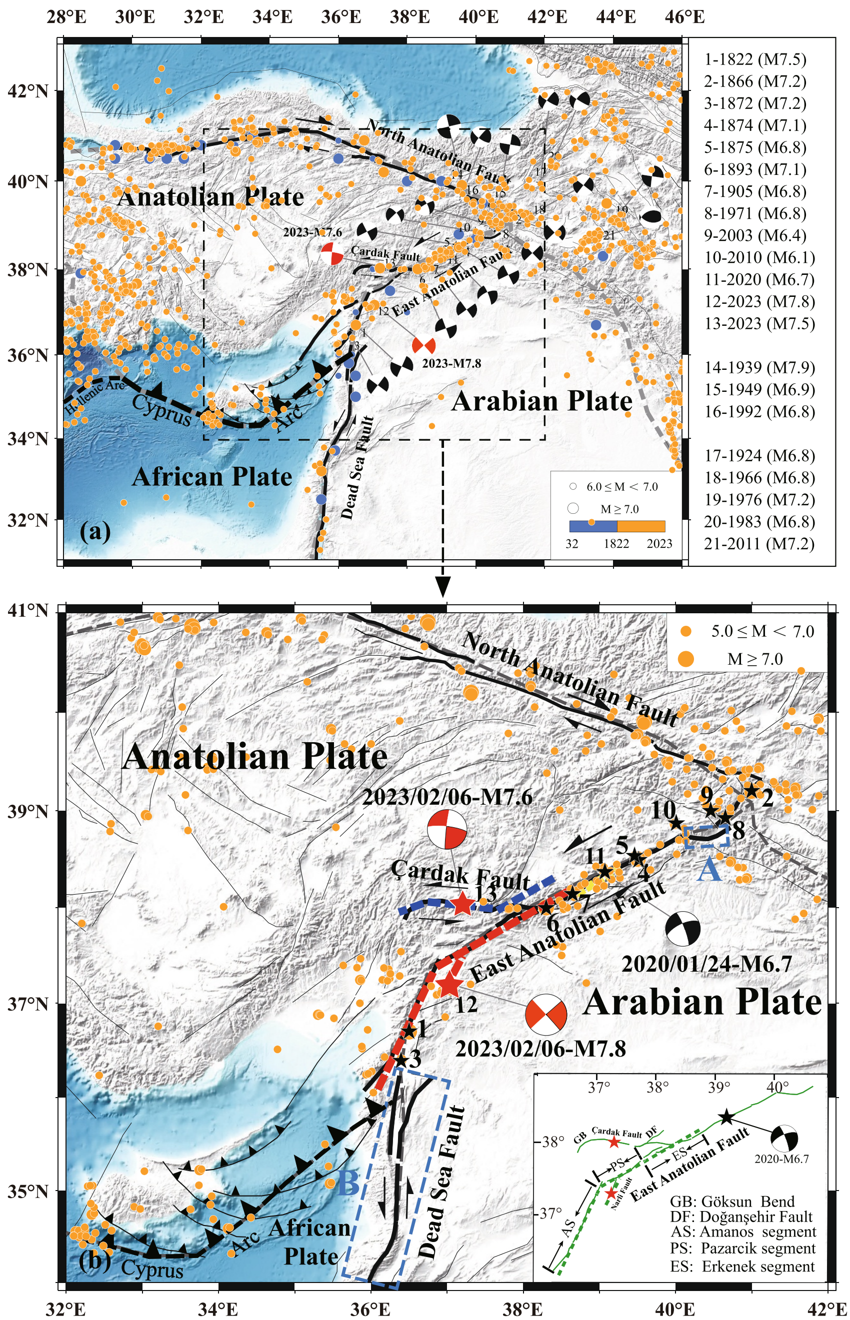

Figure 1. Geological settings of the Eastern Mediterranean area and the spatiotemporal distribution of large historical earthquakes (M ≥ 5.0) from 32 to 2023. (a) Shows the epicenters of earthquakes with blue and orange dots from 32 to 1822 and from 1822 to 2023, respectively (Ambraseys & Jackson, 1998; USGS Earthquake Hazards Program, 2017). The black stars represent the epicenters of 19 historical earthquakes (M ≥ 6.1) (Nos. 1–11 and 14–21) that occurred on and around the East Anatolian Fault (EAF) and North Anatolian Fault (NAF) from 1822 to 2022, and their focal mechanisms are shown as black beach balls. The red stars indicate the epicenters of the 2023 Mw 7.8 and Mw 7.6 earthquakes (Nos. 12 and 13), and their focal mechanisms are represented by red beach balls. The earthquake parameters are provided in Table 1. The active faults are delineated by black lines. The East Anatolian Fault, North Anatolian Fault, Cardak fault, and Dead Sea Fault (DSF) are labeled by bold black lines. The plate boundaries are delineated by bold gray dashed lines. (b) Shows the epicenters of earthquakes from 1822 to 2023. The ruptures of the 2023 Mw 7.8 and Mw 7.6 earthquakes and 2020 Mw 6.7 Elazig earthquake are illustrated as bold red, blue, and yellow dashed lines, respectively. The light blue dashed line rectangles denote seismic gaps A (Elazig-Bingol) and B in the EAF and DSF, respectively. The active fault traces are downloaded from the GEM Foundation's Global Active Faults project (https://github.com/GEMScienceTools/gem-global-active-faults). The inset shows the different segments (bold green dashed line) on the EAF. GB: Goksun bend; DF: Dogansehir Fault; AS: Amanos segment; PS: Pazarcik segment; ES: Erkenek segment.

Table 1
Information of 21 Earthquakes in and Around the EAF During the Period Between 1822 and 2023

No.	Date	Mag	Lat (N)	Lon (E)	Strike	Dip	Rake	Length (km)	Width (km)	Slip (cm)	Ref
East Anatolian Fault											
1	1822-08-13	7.5	36.7	36.5	204	90	0	140	16	500	A, B, C
2	1866-05-12	7.2	39.2	41	226	90	0	45	16	424	A, B, C
3	1872-04-03	7.2	36.4	36.5	217	90	0	34	16	313	A, B, C
4	1874-05-03	7.1	38.5	39.5	64	90	0	45	16	177	A, B, C
5	1875-03-27	6.8	38.8	39.5	243	90	0	20	16	181	A, B, C, O
6	1893-03-02	7.1	38	38.3	250	90	0	54	16	267	A, B, C, O
7	1905-12-04	6.8	38.1	38.6	234	90	0	38	16	252	A, B, C
8	1971-05-22	6.8	38.9	40.5	43	90	0	38	16	60	A, B, C
9	2003-05-01	6.4	39	40.44	154	90	−178	20	16	100	G
10	2010-03-08	6.1	38.807	40.121	54	80	−10	10	8	55	H
11	2020-01-24	6.7	38.29	39.02	240	75	−10	*	*	*	L
12	2023-02-06	7.8	37.226	37.014	228	89	−1	*	*	*	M
13	2023-02-06	7.6	38.011	37.196	277	78	4	*	*	*	M
North Anatolian Fault											
14	1939-12-26	7.9	39.8	39.3	77	90	180	25	16	150	D
					98	90	180	74	16	250	
					109	90	180	96	16	400	
					110	90	180	61	16	500	
					113	90	180	100	16	600	
15	1949-08-17	6.9	39.4	40.8	280	90	180	38	16	178	A, B, C
16	1992-03-13	6.8	39.710	39.605	126	72	172	30	15	70	K, N
Other Faults											
17	1924-09-13	6.8	40	42	215	80	10	30	16	110	E
18	1966-08-19	6.8	39.2	41.4	308	90	180	30	16	160	A, B, C
19	1976-11-24	7.2	39.1	44.02	107	78	176	14	16	250	F
					115	74	174	40	16	250	
20	1983-10-30	6.8	40.3	42.1	215	64	7	30	16	110	E
21	2011-10-23	7.2	38.76	43.36	246	46	59	*	*	*	I, J

Note. Ref indicates the references in Table 1 from which the related earthquake parameters were extracted. A: Nalbant et al., 2002; B: Ambraseys, 1989; C: Ambraseys & Jackson, 1998; D: Barka, 1996; Eyidogan & Akinci, 1999; F: Utkucu, 2013; G: Milkereit et al., 2004; H: Tan et al., 2011; I: Doğan & Karakaş, 2013; J: Irmak et al., 2012; K: Grosser et al., 1998; L: Chen et al., 2020; M: USGS Earthquake Hazards Program, 2017; N: Pinar et al., 1994; O: Taymaz et al., 1991. Asterisk (*) refers to the cited references for finite fault parameters.

processes between the six cascading sub-events during the 2023 earthquake doublet. Second, we simulated and demonstrated the stress changes along the two seismic gaps of the EAF and the DSF, discussing the potential future seismic hazards based on these stress results.

2. Geological Background and the 2023 Earthquake Doublet

The EAF is a major tectonic boundary that separates the Arabian and Anatolian plates. It formed approximately 23 million years ago due to the collision of these two plates, resulting in rapid left-lateral strike slip and the generation of large earthquakes (Dewey et al., 1986; Robertson, 2000; Taymaz et al., 1991). The 2023 Mw 7.8 earthquake occurred in the vicinity of a triple-junction between the Anatolian, Arabian, and African plates (Figure 1). Geological and geomorphological studies suggest that the slip rate of the EAF and its sub-parallel segments varies between approximately 4 mm/year and 10 mm/year from southwest to northeast along the strike (Aktug et al., 2016; Bayrak et al., 2015; Güvercin et al., 2022; Koç & Kaymakcı, 2013). The EAF has been frequently hit by devastating earthquakes throughout history, as well as during instrumental times. Between the years 1822 and 2022, 19 large earthquakes (M $\geq$ 6.1) were recorded on and around the EAF and eastern NAF (Table 1).

The reported finite fault models suggest that the 2023 Mw 7.8 earthquake consisted of three sub-events, S1–S3, which occurred on three different segments of the EAF (Barbot et al., 2023; Delouis et al., 2023; Goldberg et al., 2023; He et al., 2023; Jia et al., 2023; Li et al., 2023; Liu et al., 2023; Mai et al., 2023; Melgar et al., 2023; Okuwaki et al., 2023; Ren et al., 2024; USGS Earthquake Hazards Program, 2017; Wang et al., 2023; Xu et al., 2023; Zhang et al., 2023). Utilizing inversion based on InSAR measurements, GNSS, SM, and seismic data, USGS documented that the initial sub-event, S1, originated from the epicenter along a splay fault known as the Narli Fault (NF) of the EAF (Figures 1b and 2j), a consensus corroborated by other research (Barbot et al., 2023; Delouis et al., 2023; Goldberg et al., 2023; He et al., 2023; Jia et al., 2023; Li et al., 2023; Liu et al., 2023; Mai et al., 2023; Melgar et al., 2023; Okuwaki et al., 2023; Ren et al., 2024; Wang et al., 2023; Xu et al., 2023; Zhang et al., 2023). After about 10 s, the rupture of sub-event S1 reached the EAF and jumped to the main band of the fault, propagating bilaterally northeastwards and southwestwards along the EAF to rupture sub-events S2 and S3 (Figure 2j), respectively (USGS Earthquake Hazards Program, 2017). According to the USGS report, the S2 initiated its northeastward propagation from the conjunction between the NF and EAF along the EAF, aligning with the conclusions drawn by Barbot et al. (2023), Grabiel et al. (2023), and Jia et al. (2023) through the inversion analysis of SAR and GNSS data, as well as by Liu et al. (2023) through inversions of GNSS and SM data, and by Xu et al. (2023) through SAR, GNSS, and SM data inversion. Nevertheless, Okuwaki et al. (2023) and Ren et al. (2024) suggested an initiation point for the S2 approximately 20 and 9 km southwest, respectively, to the NF-EAF junction, based on their investigation into the dynamic rupture process of the 2023 Mw 7.8 earthquake utilizing GNSS and SM data inversion. Finally, sub-event S3 propagated southwestwards along the southwestern EAF (Amanos segment) to its southwestern end during the period of 20–90 s (USGS Earthquake Hazards Program, 2017). The dynamic rupture model suggested by Jia et al. (2023) and Gabriel et al. (2023) also reveals a 10 s delay in the onset of the SW rupture along the S3 segment with respect to the NE rupture along the S2 segment.

The rupture propagation velocity of the 2023 Mw 7.8 earthquake varies across different studies. Wang et al. (2023) and Ren et al. (2024) have posited supershear rupture occurring on S1 and a significant portion of S2, a departure from other investigations that suggested subshear rupture for both S1 and S2 (Barbot et al., 2023; Delouis et al., 2023; Gabriel et al., 2023; Goldberg et al., 2023; He et al., 2023; Jia et al., 2023; Li et al., 2023; Mai et al., 2023; Melgar et al., 2023; Okuwaki et al., 2023; Xu et al., 2023). The subshear rupture of S3, however, finds widespread agreement among previous studies (Barbot et al., 2023; Delouis et al., 2023; Goldberg et al., 2023; He et al., 2023; Jia et al., 2023; Li et al., 2023; Liu et al., 2023; Mai et al., 2023; Melgar et al., 2023; USGS Earthquake Hazards Program, 2017; Wang et al., 2023; Xu et al., 2023), with the exception being the proposals of supershear rupture or partly supershear rupture by Liu et al. (2023), Okuwaki et al. (2023), Wang et al. (2023), and Zhang et al. (2023) (Table S1 in Supporting Information S1).

The Mw 7.6 earthquake also consisted of three sub-events, S4–S6, that occurred on three separate fault segments of the CF (Figure 3l) (Barbot et al., 2023; Delouis et al., 2023; Goldberg et al., 2023; He et al., 2023; Jia et al., 2023; Li et al., 2023; Liu et al., 2023; Mai et al., 2023; Melgar et al., 2023; Ren et al., 2024; USGS Earthquake Hazards Program, 2017). According to the report by USGS, the fourth sub-event (S4) began near in the center of the CF (about 80 km long) and spread out bilaterally toward the western and eastern ends within 0–10 s. The dynamic rupture models presented by Gabriel et al. (2023), Jia et al. (2023), and Ren et al. (2024) suggest a supershear rupture propagation toward the west and subshear toward the east of S4. In contrast, Liu et al. (2023) proposed a bilateral supershear rupture propagation during the initial 8 s, transitioning to subshear rupture propagation thereafter. The fifth sub-event, S5, propagated along a fault branch called Goksun Bend (Figures 1b and 3l), which stretches for about 38 km and had a strike of 250°. This branch connects to the western end of the CF, and the rupture occurred between 15 and 30 s (USGS Earthquake Hazards Program, 2017). In the sixth sub-event, S6, the rupture propagated northeastwards along a fault branch, Doğanşehir fault (DF) (Figures 1b and 3l) between 10 and 30 s, with a length of approximately 85 km and a strike of around 60°, nearly connecting to the eastern end of the CF (Barbot et al., 2023; Delouis et al., 2023; Goldberg et al., 2023; He et al., 2023; Jia et al., 2023; Li et al., 2023; Liu et al., 2023; Mai et al., 2023; Melgar et al., 2023; Ren et al., 2024;

10.1029/2024JB029213

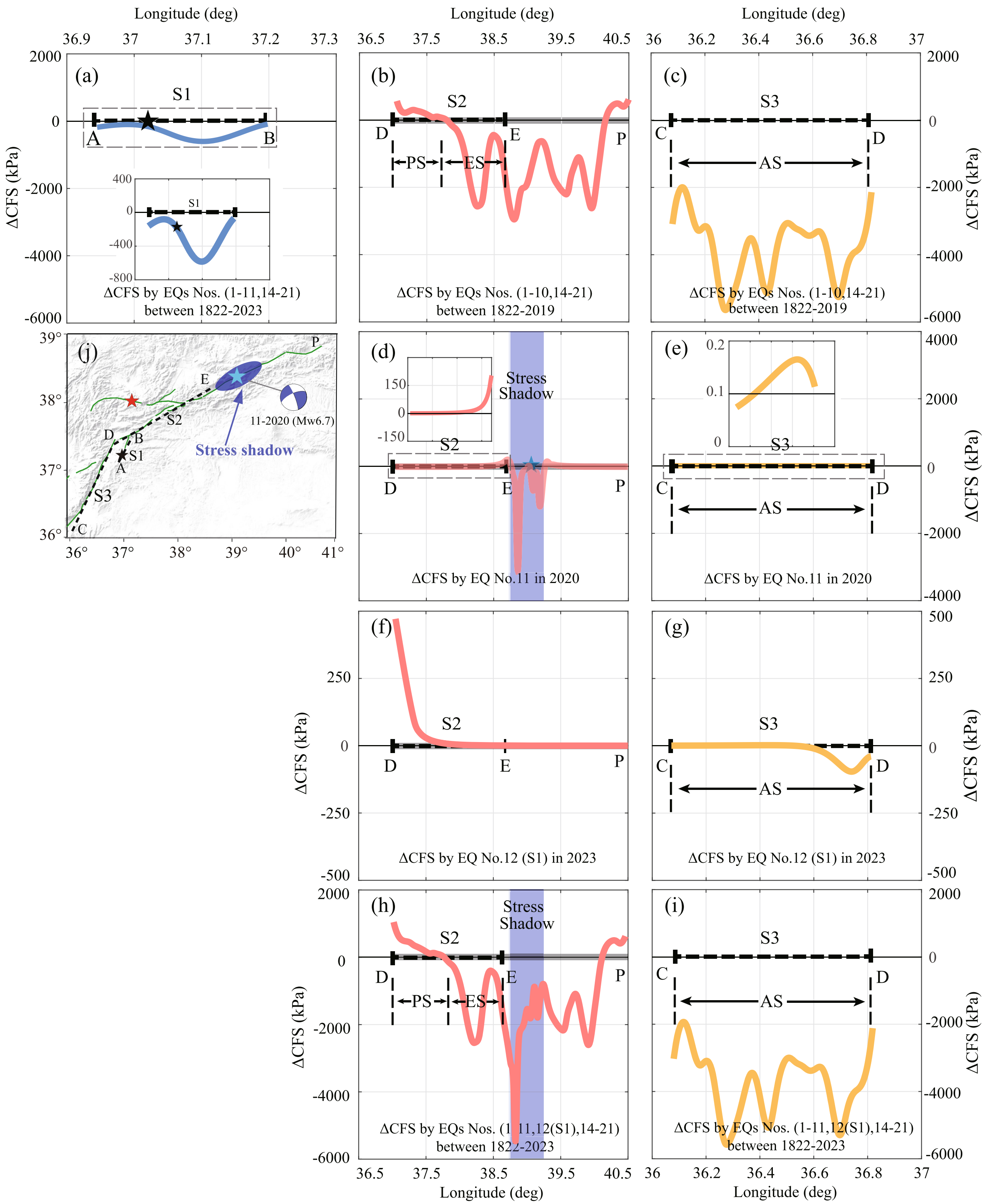

Figure 2.

USGS Earthquake Hazards Program, 2017). It should be noted that the fault slip model proposed by Okuwaki et al. (2023) does not include rupture on the S6 along the DF (Tables S1 and S2 in Supporting Information S1).

Two fault rupture models (Melgar et al., 2023; Zhang et al., 2023) propose that the rupture along the Cardak fault of the Mw 7.6 earthquake extended to the Surgu fault (lying between the Cardak fault and the EAF) and eventually reached the EAF, which is contrast to the other 14 fault rupture models detailed in Tables S1 and S2 in Supporting Information S1. Evidence from geodetic observations (Barbot et al., 2023; Gabriel et al., 2023; Li et al., 2023) and aftershock relocation (Ding et al., 2023; Melgar et al., 2023) demonstrates that the Surgu fault remained unruptured during the 2023 earthquake doublet (Figure 1b).

3. Method

According to the Coulomb failure criterion (Harris, 1998), the definition of ΔCFS is as follows:

$$\Delta \mathrm{CFS} = \Delta\tau_{\mathrm{s}} + \mu' \Delta\sigma_{\mathrm{n}}. \tag{1}$$

In the equation, $\Delta\tau_s$ and $\Delta\sigma_n$ indicate the variations in the shear stress and the normal stress, respectively. μ' is the coefficient of equivalent friction, ranging between 0.2 and 0.8.

The lithospheric model parameters were obtained from earlier seismic imaging studies (Artemieva & Shulgin, 2019; Biryol et al., 2011; Confal et al., 2018; Eken et al., 2021; Fichtner et al., 2013; Kounoudis et al., 2020; Mahatsente et al., 2018; Medved et al., 2021; Ogden & Bastow, 2022; Ozacar et al., 2010; Portner et al., 2018; Tesauro et al., 2018; Vanacore et al., 2013; Wang et al., 2020; Whitney et al., 2023; Zhu, 2018) and estimates of effective viscosity (Hearn & Bürgmann, 2005; Hearn et al., 2009; Sunbul, 2019; Sunbul et al., 2016). A summary of the parameters of the layers in the lithospheric model can be found in Table 2. The upper and lower crusts had viscosities of 1.0×10^{23} Pa.s and 1.0×10^{19} Pa.s, respectively (Hearn et al., 2009; Sunbul, 2019; Sunbul et al., 2016). Moreover, the mantle's viscosity was estimated to be 5.0×10^{18} Pa.s (Hearn et al., 2009; Sunbul, 2019; Sunbul et al., 2016). Additionally, the equivalent friction coefficient μ' was determined to be 0.4, as reported by King et al. (1994).

Fault slips of these 21 earthquakes were used as earthquake sources in the ΔCFS calculation of this study. Although fault slip models of the 2023 earthquake doublet provided by several previous studies are different in details, they share common feature in terms of multiple rupture segmentations for each main shock. In this study we used the co-seismic dislocation models of the 2023 Mw 7.8 and Mw 7.6 earthquakes (Nos. 13 and 14) provided by USGS (USGS Earthquake Hazards Program, 2017). Details regarding the size, fault slip, and rupture propagation velocity of each sub-event in the 2023 earthquake doublet are summarized in Tables S1 and S2 in Supporting Information S1. The co-seismic dislocation model of the 2020 Mw 6.7 Elazig earthquake (No. 11) was provided by Chen et al. (2020) through joint inversion of INSAR measurements, GNSS, SM, and teleseismic data.

The fault slip models of the other 18 historical earthquakes were determined by the following methods, as well-constrained co-seismic dislocations of these events are not available. The fault planes of these earthquakes are represented by rectangular planar patches with a uniform slip. The along-strike lengths, down-dip lengths, and slip magnitudes of the fault planes were estimated based on the empirical scaling laws and relationships defined by Wells and Coppersmith (1994). All these 18 historical earthquake source parameters have been successfully used in investigating the earthquake-induced stress change and crustal deformation in previous studies (Nalbant et al., 2002; Sunbul, 2019; Sunbul et al., 2016). Please refer to previous studies (Ambraseys, 1989;

Figure 2. ΔCFS distribution along the S1–S3 ruptures of the 2023 Mw 7.8 earthquake in the EAF at a 10-km depth before their respective ruptures caused by earthquakes between 1822 and 2023.The focal mechanisms of the S1-S3 used in the simulation are (strike = 28°, dip = 85°, rake = −1°), (strike = 60°, dip = 85°, rake = −1°), and (strike = 25°, dip = 75°, rake = −1°), respectively (USGS Earthquake Hazards Program, 2017). (a) ΔCFS distribution along the S1 rupture before its rupture caused by 19 historical earthquakes (Nos. 1–11, 14–21) between 1822 and 2023. (b, d, f, and h) show ΔCFS distribution along the S2 rupture before its rupture caused by 18 historical earthquakes (Nos. 1–10, 14–21) between 1822 and 2019, the 2020 Mw 6.7 Elazig earthquake (No. 11), the S1 of the 2023 Mw7.8 earthquake (No. 12(S1)), and all 20 earthquakes between 1822 and 2023 (Nos. 1–11, 12 (S1), 14–21). (c, e, g, i) show ΔCFS distribution along the S3 rupture before its rupture caused by the same earthquakes as those in figures (b, d, f, h). (j) Segments (AB, DE, and CD) indicating the faults that ruptured during the three sub-events (S1, S2, and S3, respectively) of the 2023 Mw7.8 earthquake. The blue ellipse indicates the stress shadow zone caused by the 2020 Mw 6.7 Elazig earthquake, while the black, red, and blue stars denote the epicenters of the 2023 Mw 7.8, 2023 Mw7.6, and 2020 Mw 6.7 earthquakes, respectively. Amanos, Erkenek, and Pazarcik segments are abbreviated as AS, ES, and PS, respectively.

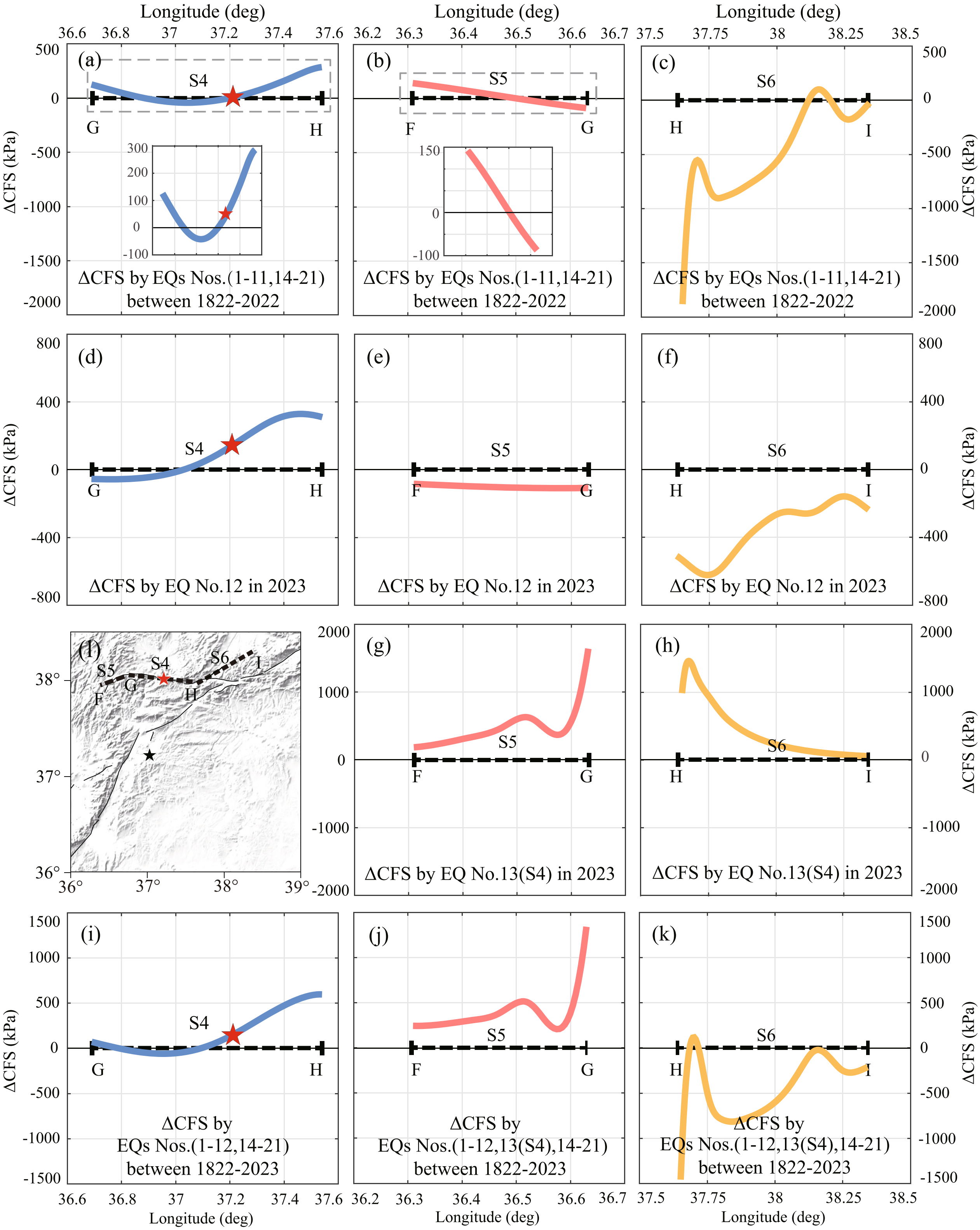
Longitude (deg)
ΔCFS (kPa)
(a)
S4
G
H
ΔCFS by EQs Nos.(1-11,14-21) between 1822-2022
(b)
S5
F
G
ΔCFS by EQs Nos.(1-11,14-21) between 1822-2022
(c)
S6
H
I
ΔCFS by EQs Nos.(1-11,14-21) between 1822-2022
(d)
ΔCFS by EQ No.12 in 2023
(e)
ΔCFS by EQ No.12 in 2023
(f)
ΔCFS by EQ No.12 in 2023
(f)
S5
S4
S6
F
G
H
I
(g)
ΔCFS by EQ No.13(S4) in 2023
(h)
ΔCFS by EQ No.13(S4) in 2023
(i)
ΔCFS by EQs Nos.(1-12,14-21) between 1822-2023
(j)
ΔCFS by EQs Nos.(1-12,13(S4),14-21) between 1822-2023
(k)
ΔCFS by EQs Nos.(1-12,13(S4),14-21) between 1822-2023

Figure 3.

Ambraseys & Jackson, 1998; Chen et al., 2020; Güvercin et al., 2022) for the detailed information of the historical earthquakes (Nos. 1–11, 14–21 in Figure 1) between 1822 and 2022. The earthquake parameters are listed in Table 1, and a total of 21 earthquakes were analyzed using the ΔCFS calculation.

Assuming viscoelastic rheology in the lithosphere of the eastern Anatolian Plate, we used the PSGRN/PSCMP code (Wang et al., 2003, 2006) to calculate the earthquake stress caused by the dislocation sources in the layered gravitational lithospheric model. More details about the ΔCFS calculation and PSGRN/PSCMP code, please refer to the previous publications by Wang et al. (2003, 2006) and Shi and Cao (2010). We calculated the ΔCFS values at a 10-km depth, near the hypocenter depth recommended by USGS, considering both co-seismic stress changes and post-seismic stress relaxation until 2023 caused by a total of 21 earthquakes in and around the EAF from 1822 to 2023. The focal mechanism of the receiver faults of different sub-events of the 2023 earthquake doublet or segments in EAF and DSF used in the calculation is listed in Table 3.

4. Results and Discussion

4.1. The Delayed Mw 7.8 Earthquake

The initiation point of the Mw 7.8 earthquake's first sub-event (S1) (segment AB in Figures 2a and 2j) was not on the main strand of the EAF but on a splay fault (Narli fault) (Barbot et al., 2023; Delouis et al., 2023; Goldberg et al., 2023; He et al., 2023; Jia et al., 2023; Li et al., 2023; Liu et al., 2023; Mai et al., 2023; Melgar et al., 2023; Okuwaki et al., 2023; Ren et al., 2024; USGS Earthquake Hazards Program, 2017; Wang et al., 2023; Xu et al., 2023). Our results showed a release of stress over the entire S1 rupture, with a minimum ΔCFS of −584 kPa prior to the 2023 Mw 7.8 earthquake, due to 19 historical earthquakes (Nos. 1–11, 14–21) between 1822 and 2022 (Figure 2a). A decrease of −154 kPa in ΔCFS was observed at the hypocenter (Figure 2a), which was mainly contributed by the 1822 M 7.5 (No. 1) (Text S4.1 in Supporting Information S1). Stress shadow effects inhibiting earthquake activity have been observed in previous studies, such as those on the San Andreas Fault system (Freed & Lin, 2001; Harris, 1998; Harris & Simpson, 1996; Mallman & Parsons, 2008; Simpson et al., 1988), central Sulawesi (Liu & Shi, 2021), eastern Tibet (Liu et al., 2018, 2020), northeastern Tibet (Chen et al., 2022; Liu et al., 2022), and southern Tibet (Gahalaut et al., 2011). We suggest that the unloaded stress on the earthquake hypocenter, resulting from historical earthquake interactions in the EAF over the past two centuries, likely delayed the S1 rupture of the 2023 Mw 7.8 earthquake. Based on the interseismic tectonic loading Coulomb stressing rate of 3 kPa/y (Sunbul, 2019), the ΔCFS of 154 kPa was equivalent to tectonic loading for approximately 52 years.

The viscoelastic effect on the stress results was also examined (Text S7 in Supporting Information S1). The findings show that the cumulative ΔCFS at the hypocenter of the 2023 Mw 7.8 earthquake increased from −557 kPa to −154 kPa from the co-seismic to post-seismic levels until 2023 caused by 19 historical earthquakes (Nos. 1–11, 14–21) between 1822 and 2022 (Figure S31 in Supporting Information S1). Based on the interseismic tectonic loading Coulomb stressing rate of 3 kPa/year (Sunbul, 2019), the ΔCFS increment of 403 kPa, due to viscoelastic stress relaxation in the ductile layers of the Anatolian Plate, is equivalent to approximately 134 years of tectonic loading. This highlights the significant contribution of viscous rebound to the 2023 Mw 7.8 earthquake. The phenomenon of viscous rebound caused by ductile lithospheric layers accelerating earthquakes is not unique to the EAF. Similar effects have been observed in the 1999 Hector Mine earthquake in southern California (Freed & Lin, 2001; Pollitz & Sacks, 2002; Zeng, 2001), the 2008 Wenchuan Mw 7.9 earthquake in eastern Tibet (Liu et al., 2017b), and the earthquake sequence in the Musgrave block of Central Australia (Mohammadi, 2022).

Figure 3. ΔCFS distribution along the S4–S6 ruptures of the 2023 Mw 7.6 earthquake in the CF at a 10-km depth before their respective ruptures caused by earthquakes between 1822 and 2023. The focal mechanisms of the S4–S6 used in the simulation are (strike = 276°, dip = 80°, rake = −1°), (strike = 250°, dip = 80°, rake = −1°), and (strike = 60°, dip = 80°, rake = −1°), respectively (USGS Earthquake Hazards Program, 2017). (a, d, i) show ΔCFS distribution along the S4 rupture before its rupture caused by 19 historical earthquakes (Nos. 1–11, 14–21) between 1822 and 2022, the 2023 Mw7.8 earthquake (No. 12), and all 20 earthquakes between 1822 and 2023 (Nos. 1–12, 14–21). (b, e, g, j) show ΔCFS distribution along the S5 rupture before its rupture caused by 19 historical earthquakes (Nos. 1–11, 14–21) between 1822 and 2022, the 2023 Mw7.8 earthquake (No. 12), the S4 of the Mw7.6 earthquake (No. 13(S4)), and all 21 earthquakes between 1822 and 2023 (Nos. 1–12, 13(S4), 14–21). (c, f, h, k) show ΔCFS distribution along the S6 rupture before its rupture caused by the same earthquakes as those in figures (b, e, g, j). (l) Segments (GH, GF, and HI) indicating the faults that ruptured during the S4, S5, and S6, respectively, of the 2023 Mw7.6 earthquake. The black and red stars denote the epicenters of the 2023 Mw 7.8 and Mw7.6 earthquakes, respectively.

Table 2
The Layer Parameters in the Lithospheric Model

Layers	H (km)	ρ (kg/m³)	Vp (km/s)	Vs (km/s)	η (Pa.s)
UC	0 ~ −20	2570	6.10	3.60	1.0×10^{23}
LC	−20 ~ −40	2830	7.20	4.20	1.0×10^{19}
LM	−40 ~ −100	3,370	7.71	4.51	5.0×10^{18}

Note. H is the depth (Ogden & Bastow, 2022; Tesauro et al., 2018), Vp and Versus are the compression and shear waves velocities, respectively (Artemieva & Shulgin, 2019, 2020; Biryol et al., 2011; Confal et al., 2018; Eken et al., 2021; Fichtner et al., 2013; Kounoudis et al., 2018, 2020; Mahatsente et al., 2018; Medved et al., 2021; Ogden & Bastow, 2022; Ozacar et al., 2010; Portner et al., 2018; Tesauro et al., 2018; Vanacore et al., 2013; Zhu, 2018; Wang et al., 2020; Whitney et al., 2023), and η is the viscosity (Hearn & Bürgmann, 2005; Hearn et al., 2009; Sunbul, 2019; Sunbul et al., 2016). UC: upper crust; LC: lower crust; LM: lithospheric mantle.

4.2. Deciphering the Mw 7.8 Earthquake Rupture Propagation and Termination

Our results show that stress in the Pazarcik segment (PS in Figure 2b) of the second sub-event (S2) rupture is increased with the maximum ΔCFS value of 593 kPa at the very southwestern end prior to its rupture caused by 18 earthquakes (Nos. 1–10, 14–21) between 1822 and 2019 (Figure 2b). This result is consistent with previous findings of loaded stress on the Pazarcik segment by the same 18 historical earthquakes before 2019 (Nos. 1–10, 14–21) (Sunbul, 2019). Moreover, we assess the stress change on the S2 rupture caused by the 2020 Mw 6.7 Elazig earthquake (No. 11) (Figure 2d) and the S1 of the 2023 Mw 7.8 earthquake (No. 12 (S1)) (Figure 2f), which were not included in previous stress calculations (Nalbant et al., 2002; Sunbul, 2019).

Our analysis shows that the already stressed Pazarcik segment on the S2 rupture is further stress-promoted, reaching a maximum static stress value of approximately 471 kPa at its southwestern end prior to its rupture, caused by the S1 event (Figure 2f). Based on the interseismic tectonic loading Coulomb stressing rate of 3 kPa/y (Sunbul, 2019), the ΔCFS of 471 kPa is equivalent to tectonic loading for approximately 157 years, signaling strong physical connection between the S1 and S2. Therefore, we suggest that the S1 triggered the S2, resulting in its northeastward rupture propagation along the Pazarcik segment of the EAF. Previous studies indicate that dynamic stresses are likely to play a significant role in triggering events, as rupture velocities approach or exceed the shear wave speed (Aochi et al., 2000; Kame et al., 2003; Yamashita & Umeda, 1994). The supershear rupture on the S1 was identified by Ren et al. (2024) and Wang et al. (2023) through their investigation of the dynamic rupture process of the 2023 earthquake doublet. Ren et al. (2024) suggest that the peak dynamic Coulomb stress (1,400 kPa) at the initiation point of the S2 was caused by the initial rupture of S1. This implies that the rupture of the S1 may also play a crucial role in triggering and facilitating the rupture of S2 on the Pazarcik segment through dynamic stress triggering (Gabriel et al., 2023; Ren et al., 2024). These findings underscore the significance of examining the influence of the initial rupture on branch fault triggering rupture on the main fault, leading to large continental earthquakes by augmenting both static and dynamic stress, as observed in events like the 2001 Kokoxili Mw 7.9 earthquake on the east Kunlun fault in northern Tibet, the 2002 Denali Mw 7.9 earthquake on the Denali fault in Alaska (Hreinsdottir et al., 2003; Lasserre et al., 2005), and the 1812 M7.5 earthquake on the San Andreas fault and San Jacinto Fault system in California (Lozos, 2016; Xu et al., 2023).

A notable stress shadow is observed to the northeastern end of the S2 rupture of the 2023 Mw 7.8 earthquake, with a minimum ΔCFS of approximately −5461 kPa (Figure 2h), primarily induced by the 2020 Mw 6.7 Elazig earthquake (Figure 2d), consistent with the stress change estimated by Toda and Stein (2024). This stress shadow has the potential to impede the northeastward extension of rupture for the 2023 Mw 7.8 event and confine its aftershock distribution to the northeast (as indicated by the light blue dots in Figure S29 in Supporting Information S1), consistent with the established stress shadow theory applied in other fault zones (Chen et al., 2022; Freed & Lin, 2001; Harris, 1998; Harris & Simpson, 1996; Liu et al., 2018, 2020, 2022; Liu & Shi, 2021; Mallman & Parsons, 2008; Simpson et al., 1988). Similarly, we found that the 2020 earthquake's rupture and aftershock distribution were confined within an area of stress increase, bounded by stress shadows from the 1874 and 1905 events (Figure S28c in Supporting Information S1).

Table 3
Focal Mechanism of the Receiver Faults of Different Sub-Events of the 2023 Earthquake Doublet or Segments in the EAF and DSF (Figures 1b, 2j and 3l, and 5) (USGS Earthquake Hazards Program, 2017)

								Seismic gap B		
Focal mechanism	S1	S2	S3	S4	S5	S6	Seismic gap A	LM	NO	QR
Strike	28°	60°	25°	276°	250°	60°	70°	190°	210°	180°
Dip	85°	85°	75°	80°	80°	80°	85°	75°	70°	85°
Rake	−1°	−1°	−1°	−1°	−1°	−1°	−1°	25°	−40°	15°

10.1029/2024JB029213

These observations of stress shadow effects and their impact on earthquake rupture termination are consistent globally, as demonstrated in the Logmen Shan fault in eastern Tibet during the 2008 Mw 7.9 Wenchuan earthquake, the northeastern Tibet during the 2021 Mw 7.3 Maduo and 2022 Mw 6.6 Menyuan earthquakes (Liu & Shi, 2021, 2022), and the Palu-Koro fault in Central Sulawesi, Indonesia, during the 2018 Mw 7.5 Palu earthquake (Liu et al., 2018, 2020). These insights contribute to a broader understanding of earthquake rupture propagation and termination, as exemplified by the unilaterally eastward rupture in the 2002 Mw 7.9 Denali fault earthquake (Eberhart-Phillips et al., 2003; Hreinsdóttir et al., 2003).

4.3. The Triggered Mw 7.6 Earthquake

The initiation point of the Mw 7.6 earthquake was on the middle of the CF (segment GH in Figures 3a and 3l) (Barbot et al., 2023; Delouis et al., 2023; Goldberg et al., 2023; He et al., 2023; Jia et al., 2023; Li et al., 2023; Liu et al., 2023; Mai et al., 2023; Melgar et al., 2023; Okuwaki et al., 2023; Ren et al., 2024; USGS Earthquake Hazards Program, 2017; Xu et al., 2023). Our research demonstrates that stress is increased almost over the entire fourth sub-event (S4) rupture (segment GH in Figure 3l) caused by early earthquakes before its rupture (Figure 3i). We find that the increased ΔCFS value of 78 and 252 kPa on the hypocenter of the Mw 7.6 earthquake is caused by 19 historical earthquakes (Nos. 1–11, 14–21) (Figure 3a) between 1822 and 2022 and the 2023 Mw 7.8 earthquake (No. 12) (Figure 3d), respectively. Our discovery of an elevated ΔCFS value of 252 kPa in the epicentral region of the Mw 7.6 earthquake caused by the 2023 Mw 7.8 earthquake (No. 12) closely aligns with the estimates of 200 kPa by He et al. (2023) and the range of 140∼189 kPa proposed by Liu et al. (2023). However, it significantly deviates from the value of 40 kPa suggested by Okuwaki et al. (2023) and falls below the estimate of 300 kPa by Toda and Stein (2024) and several hundred kPa by Jia et al. (2023). These variations can be attributed to differences in methodologies, earthquake parameters, and slip models employed across various studies when assessing earthquake-induced stress changes. Given the interseismic tectonic loading Coulomb stressing rate of 3 kPa/y (Sunbul, 2019), the ΔCFS of 78 and 252 kPa corresponds to tectonic loading for approximately 26 and 75 years, respectively. Thus, we suggest that the historical earthquake activities between 1822 and 2022 bring the CF close to failure, with a loaded stress on the S4 rupture equivalent to approximately 26 years of tectonic loading. The 2023 Mw 7.8 earthquake adds further stress to the S4 rupture, ultimately triggering the 2023 Mw 7.6 earthquake by advancing it for approximately 75 years. Note that the 2023 Mw 7.6 earthquake occurred approximately 9 hr after the Mw 7.8 earthquake (USGS Earthquake Hazards Program, 2017). Despite encountering a significant transient increase in dynamic Coulomb stress of several megapascals due to the passage of seismic waves, the 2023 Mw 7.8 earthquake did not promptly trigger the occurrence of the 2023 Mw 7.6 earthquake (Gabriel et al., 2023; Jia et al., 2023; Ren et al., 2024). Combining with our results, it suggests that the triggering mechanism between the Mw 7.8 and 7.6 earthquakes is likely related to static stress rather than dynamic stress, given that the events were separated by a time interval of 9 hr. Note that other processes, such as early aseismic slip, poroelastic rebound by increase of permeability, and normal stress change caused by the Mw 7.8 earthquake, could also help to explain the triggering (Manga et al., 2012; Rojstaczer et al., 1995; Shaddox et al., 2021; Toda & Stein, 2024). This underscores the imperative for deeper research aimed at deciphering the role of stress changes on earthquake triggering in the future.

4.4. Interplay Between Sub-Events by Stress Triggering and Shadow

We find that the fifth sub-event (S5) rupture segment (GF in Figures 3b and 3l) is largely brought away from failure due to stress unloading, with a minimum ΔCFS value of approximately −197 at its northeastern end (point G in Figure 3l) prior to the 2023 Mw 7.6 earthquake caused by 19 historical earthquakes (Nos. 1–11, 14–21) (Figure 3b) and the 2023 Mw 7.8 earthquake (No. 12) (Figure 3e). This is consistent with previous findings regarding the influence of the 2023 Mw 7.8 earthquake on S5 (Toda & Stein, 2024). However, it is brought back to failure by the S4 of the Mw 7.6 earthquake (No. 13 (S4)) due to stress loading over the entire S5 rupture, with the highest ΔCFS value of approximately 1647 kPa at its northeastern end (Figure 3g). We believe that the S5 was 1450 kPa or less (the net ΔCFS effect from previous events) far from failure and that likely loading from the rupture on the S4 segment has been meaningful to produce its final rupture.

The S6 rupture (HI in Figures 3c and 3l) is also stress unloaded, with a minimum ΔCFS value of approximately −2502 kPa at its southwestern end (point H in Figure 3l), due to the same 20 earthquakes (Nos. 1–12, 14–21) (Figures 3c and 3f). Although the S4 increases stress over the entire S6 rupture, with the highest ΔCFS value of 1279 kPa at its southwestern end (Figure 3h), this positive stress is not sufficient to compensate for the negative stress caused by the 20 historical earthquakes (Nos. 1–12, 14–21) and bring the S6 rupture segment back to failure. Finally, the entire S6 rupture is located in the stress shadow, with the minimum ΔCFS value of approximately −1457 kPa observed at its southwestern end before its rupture (Figure 3k). Similarly, we find that the Amanos segment (CD in Figure 2j) of the S3 rupture is also located in the stress shadow, with a minimum ΔCFS value of approximately −5,574 kPa, before its rupture due to unloaded stress by historical earthquakes between 1822 and 2023 (Figure 2i).

These results indicate that the intricate interplay among the six sub-events through stress triggering and shadow effects during the 2023 earthquake doublet is a complex phenomenon. Notably, the preceding sub-event not only serves to promote the subsequent sub-events but also demonstrates a propensity to delay such events. This observation aligns with prior proposals which suggest that a stress change occurring along a fault can give rise to the promotion or delay of an induced instability on the secondary fault (Belardinelli et al., 2003). Based on our observations of positive stress transfer between the S1 and S2, S4 and S5, and S4 and S6, with the maximum ΔCFS values of 471 kPa, 1647 kPa, and 1279 kPa, respectively, we propose that stress changes induced by preceding sub-events play a significant role in promoting rupture propagation of subsequent sub-events and its migration between multiple segments during the 2023 earthquake doublet. Nevertheless, the impact of static stress change resulting from interactions between cascading sub-events and its influence on the initiation and propagation of earthquake sequences or doublets has been largely overlooked in the past.

It is important to point out that the factors that control the initiation of those sub-events located in the stress shadow, such as the S1 (Figure 2a), the Erkenek segment of the S2 (Figure 2h), the S3 (Amanos segment) (Figure 2i), and the S6 (Figure 3k), remain unclear. Note that fault rupture initiation and propagation are significantly influenced by the stress on the fault prior to its ultimate rupture (Duan, 2010; Duan & Oglesby, 2006; Liu, Zhu, Yang, & Shi, 2016, Liu et al., 2018; Payne & Duan, 2015; Wen et al., 2012). The stress evolution before and during an earthquake sequence or doublet, rupturing several segments in a complex fault system, is complicated. The stress level on the first sub-event is mainly controlled by inter-seismic tectonic stress accumulation (Duan & Oglesby, 2005, 2006, 2007; Liu, Zhu, Yang, & Shi, 2016, 2016b, 2017b), stress change induced by previous historical earthquakes on and nearby the target fault (Chen et al., 2022; Harris, 1998; Liu et al., 2017a, 2018, 2020, 2022; Reasenberg & Simpson, 1992; Stein, 1999), and post-seismic viscous rebound (Freed, 2005; Liu et al., 2022; Mohammadi, 2022; Zeng, 2001). In contrast, stress on subsequent sub-events requires extra consideration of both static and dynamic stress changes induced by preceding sub-events during the earthquake sequence or doublet (Antonioli et al., 2002; Belardinelli et al., 1999, 2003; Ren et al., 2024; Taufiqurrahman et al., 2023).

Our results provide a unified interpretation on the static stress change on each sub-event induced by the previous earthquakes ruptures (between 1822 and 2023) before their corresponding ruptures. Strong earthquake-induced stress variation along the segments of the six sub-events was observed prior to their corresponding ruptures (Figure 6a). The stress shadow effect was most pronounced on the S1 (NF), the Erkenek segment of the S2, the S3 (Amanos segment), and the S6 (DF), reaching minimum values of −584 kPa, −1,036 kPa, −5,574 kPa, and −1,457 kPa, respectively, before their corresponding rupture (Figure 6a). These findings suggest that the accumulation of tectonic loading stress over an earthquake cycle in the EAF, coupled with the dynamic stress change induced by preceding sub-events during the 2023 earthquake doublet, may have played significant roles in initiating these sub-events. However, the dynamic stress changes on the Erkenek segment of the S2, the S3, and the S6 segments, which might partially compensate for the negative stress induced by previous events, remain unclear. Further research should investigate the dynamic stress changes on each sub-event segment of the 2023 earthquake doublet during its rupture process. It should be noted that the fault slip model proposed by Okuwaki et al. (2023) does not include rupture on the S6 along the DF (Tables S1 and S2 in Supporting Information S1).

Notably, previous research indicated that the maximum tectonic loading ΔCFS can accumulate to approximately 11 MPa over a recurrence interval of around 6,000 years of the 2008 Wenchuan Mw 7.9 earthquake on the Longmen Shan fault zone in eastern Tibet (Liu, Zhu, Yang, & Shi, 2016, Liu et al., 2017b). Additionally, investigations into the 2019 Ridgecrest Mw 7.1 earthquake rupture sequence in California estimated a maximum dynamic shear stress of approximately 2 MPa (Taufiqurrahman et al., 2023). However, the inter-seismic tectonic stress accumulation in the seismogenic depth preceding the 2023 earthquake doublet remains unclear. To gain a better understanding of the reasons behind the rupture initiation of those sub-events such as the S1, S3, and S6, future research should prioritize investigating the accumulation of inter-seismic tectonic loading stress on the seismogenic depth of the EAF and CF.

10.1029/2024JB029213

Overall, in this study we reveal how the stress changes induced by preceding sub-events can influence the occurrence and behavior of subsequent sub-events with the example of the 2023 earthquake doublet. This is important for us to understand the role of earthquake-induced stress change on earthquake dynamics across various time scales from seconds to hours and years at different stages of an earthquake cycle, including earthquake preparation, rupture initiation, propagation, and termination on multiple fault segments in structurally complex fault systems worldwide, such as the Mw 7.1 earthquake in Pakistan (Nissen et al., 2016), the 2004 Chuetsu earthquake in Niigata, Japan (Hikima & Koketsu, 2005), the 2009 Mw 8.1 Tonga-Samoa earthquake in the Tonga subduction zone (Fan et al., 2016), the 2012 great Mw 8.7 intraplate earthquake and the great Mw 8.2 aftershock in southwest of the Sumatra subduction zone (Yue et al., 2012), the 2019 Mw 7.1 Ridgecrest earthquake in the Eastern California Shear Zone (Ramos et al., 2020; Taufiqurrahman et al., 2023), and the 2016 Mw 7.8 Kaikōura earthquake in the Marlborough fault system in southern New Zealand (Ulrich et al., 2019).

4.5. Raised Hazards and Seismic Gaps

Our study, drawing from a wide array of paleoearthquake data and fault slip models (Ambraseys, 1989; Ambraseys & Jackson, 1998; Duman & Emre, 2013; Guvercin et al., 2022; Jia et al., 2023; Melgar et al., 2023; Okuwaki et al., 2023; Tan et al., 2011; USGS Earthquake Hazards Program, 2017), identifies a critical seismic gap of approximately 70 km on the northeastern EAF, known as the Elazig-Bingol seismic gap (Figure 1). Although Nalbant et al. (2002) and Sunbul (2019) have computed the stress changes in various sections of the EAF induced by 18 historical earthquakes occurring before 2019 (Nos. 1–10, 14–21), notably, the stress change in this seismic gap (between Palu and Ilica cities) remains unaddressed. Our results show that this gap has endured significant stress loading from 18 historical earthquakes (Nos. 1–10, 14–21) between 1822 and 2019 (Figure 4a), the 2020 Mw 6.7 Elazig earthquake (No. 11) (Figure 4b), and the consequential 2023 Mw 7.8 and Mw 7.6 earthquakes (Nos.12 and 13) (Figures 4c and 4d), resulting in maximal ΔCFS values of 1541 kPa, 3 kPa, 7 kPa, and 4 kPa, respectively. With an interseismic tectonic loading Coulomb stressing rate of 3 kPa/y (Sunbul, 2019), the maximal accumulated ΔCFS of 1547 kPa equates to approximately 516 years of tectonic loading (Figure 4e). Given the absence of a major earthquake in this gap for several centuries (Guvercin et al., 2022; Nalbant et al., 2002; Sunbul, 2019), the increasing stress underscores the potential for future seismic events. Should the entire 70 km segment rupture, we anticipate an earthquake exceeding 7.3 magnitude, releasing energy accumulated at a fault slip rate of about 10 mm/yr over the last century (Aktug et al., 2016; Bayrak et al., 2015; Koç & Kaymakcı, 2013). Therefore, focused attention is warranted for the areas between Palu and Ilica cities within the Elazig-Bingol seismic gap of the EAF. Using near-field geodetic data from the rupture zone of the 2020 Elazıg earthquake, Cakir et al. (2023) unveil shallow creep along the fault zone, which impeded earthquake rupture propagation and mitigated the 2020 earthquake magnitude. The prevalence and persistence of shallow creep processes across various sections of the EAF remain uncertain. Clarifying this aspect is crucial for earthquake forecasting and estimating future seismic hazards along the EAF. To improve the evaluation of the hazard potential within the Elazig-Bingol seismic gap, it is imperative for future research to concentrate on detecting and understanding fault creep behavior in this region.

Another seismic gap in the northern section of the DSF, designated as zone B in Figure 1, has not witnessed a major earthquake for over 830 years, despite multiple large earthquakes ($M > 7.0$) occurring between 859 AD and 1408 AD (Dal Zilio & Ampuero, 2023; Meghraoui et al., 2003). This gap, located in a densely populated region spanning southeastern Türkiye, northern Syria, and Lebanon, has seen varied stress alterations. Our findings revealed that while stress was decreased over half of segment LM (with a minimum ΔCFS value of approximately −504 kPa), it was increased over most of segments NO and QR, with a maximum ΔCFS value of about 312 kPa (Figure 5d). This stress increment was principally induced by two historical earthquakes (Nos. 1 and 3) on the Amanos segment of the EAF (Figure 5a), alongside contributions from the 2023 earthquake doublet, further increasing stress on segments NO and QR by about 10 kPa (Figures 5b and 5c). Consequently, the heightened seismic hazards in the seismic gap of the northern portion of the DSF merit urgent attention.

The 2023 earthquake doublet, involving multiple faults through distinct slip episodes, underscores the complex, interconnected nature of seismic processes across varying temporal and spatial scales. Early reports of this doublet (Jia et al., 2023) indicate a substantial augmentation in both rupture length and seismic moment relative to historical earthquakes in the region. Our study leverages an integrative approach, combining seismic observations, historical seismicity data, and earthquake stress change simulations to illustrate how fault interactions contributed to a cascade of ruptures. Incorporating methodologies like those presented in this study could enhance

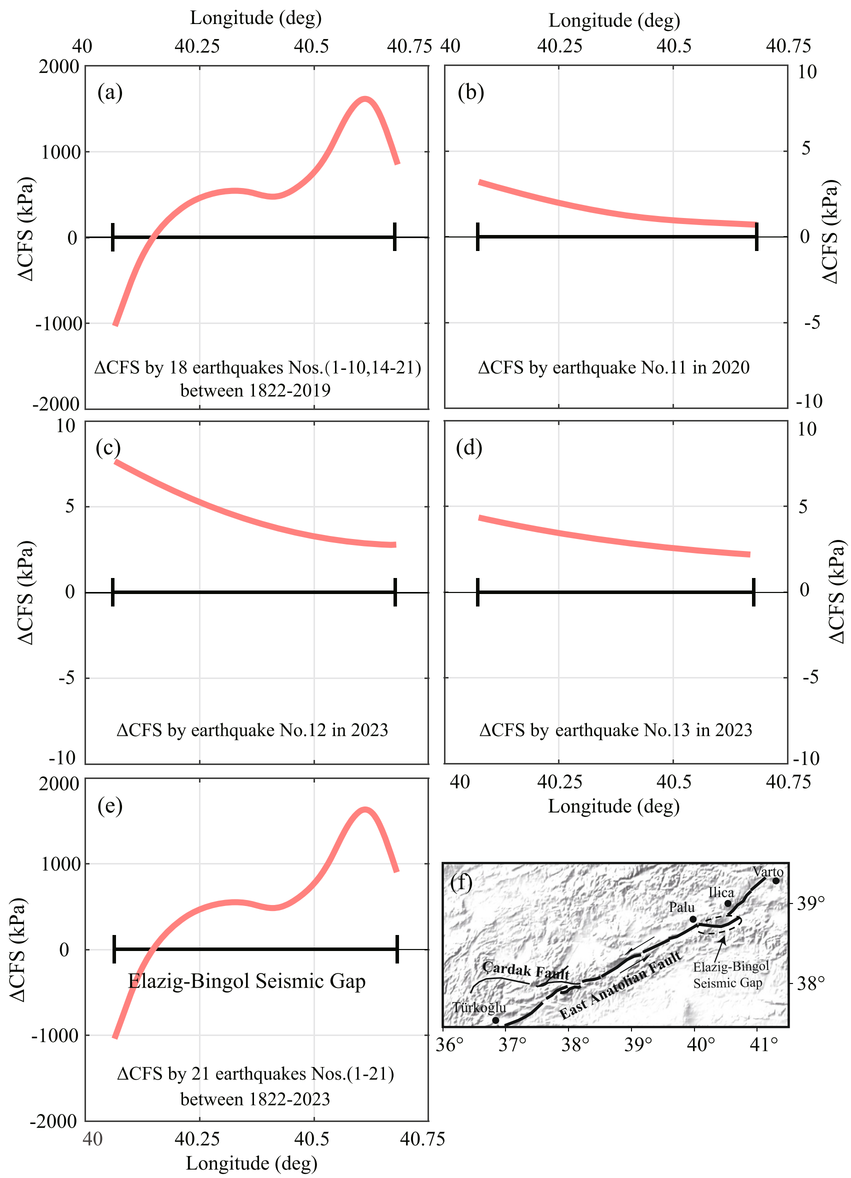

Figure 4. ΔCFS distribution along the seismic gap Elazig-Bingol in the EAF at a 10-km depth after 2023. The focal mechanism used in the simulation is (strike = 70°, dip = 85°, rake = −1°). ΔCFS was caused by (a) 18 historical earthquakes (Nos. 1–10, 14–21) between 1822 and 2019, (b) the 2020 Mw 6.7 Elazig earthquake (No. 11), (c) the 2023 Mw 7.8 earthquake (No. 12), (d) the 2023 Mw 7.6 earthquake (No. 13), and (e) all the 21 historical earthquakes (Nos. 1–21) between 1822 and 2023. (f) The location of the Elazig-Bingol seismic gap in the EAF. The black dots show cites (Palu, Ilica, and Varto) with names.

the earthquake forecasting capabilities, thereby improving decision-making processes in disaster management and rapid earthquake response scenarios.

4.6. Sensitivity of Stress Results

Varying the source location and slip of the historical earthquakes, as well as the viscosity of the ductile layers in the lithosphere, does not alter the overall earthquake-induced stress pattern and sign of stress for each of the sub-events (S1–S6), except in four specific cases, according to our sensitivity test (Text S4 in Supporting Information S1). However, it has impacts on the stress value on the target faults to some extent. Taken as examples, by considering the uncertainty from all the cases by model parameterization, including the 1822 M 7.5 (No. 1), 1866 M7.2 (No. 2), 1872 M 7.2 (No. 3), 1874 M7.1 (No. 4), 1893 M7.1 (No. 6), 1905 (No. 7), and 1971 M 6.8 (No. 8)

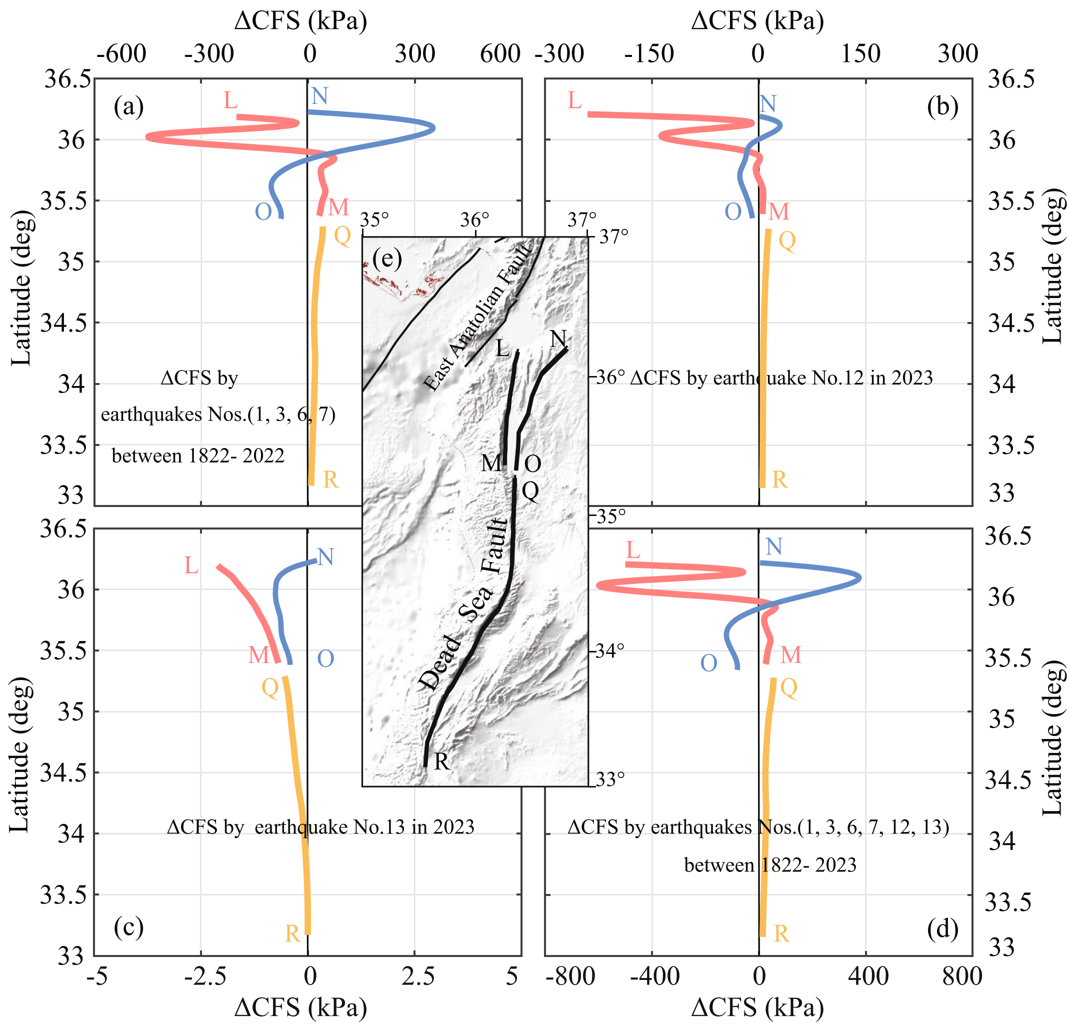

Figure 5. ΔCFS distribution along different segments of the seismic gap in the northern portion of the DSF at a 10-km depth after 2023. The focal mechanisms of segments LM, NO, and QR used in simulation are (strike = 190°, dip = 75°, rake = 25°), (strike = 210°, dip = 70°, rake = −40°), and (strike = 180°, dip = 85°, rake = 15°), respectively. ΔCFS was caused by (a) 4 historical earthquakes (Nos. 1, 3, 6, and 7) between 1822 and 2022, (b) the 2023 Mw 7.8 earthquake (No. 12), (c) the 2023 Mw 7.6 earthquake (No. 13), and (d) all the six historical earthquakes (Nos. 1, 3, 6, 7, 12, and 13) between 1822 and 2023. (e) The locations of the different segments AB, CD, and EF in the northern section of the DSF.

earthquakes source parameters, and the viscosities of the lower crust and lithospheric mantle, we found that the negative ΔCFS on the 2023 Mw 7.8 earthquake epicenter caused by 19 historical earthquakes (Nos. 1–11, 14–21) between 1822 and 2023 ranged from −509 to −103 kPa. The positive ΔCFS caused by 19 historical earthquakes (Nos. 1–11, 14–21) between 1822 and 2022 ranged from 32 to 130 kPa on the 2023 Mw 7.6 earthquake epicenter. Based on the interseismic tectonic loading Coulomb stressing rate of 3 kPa/y (Sunbul, 2019), the ΔCFS of 509, 103, 32, and 130 kPa was equivalent to tectonic loading for approximately 169, 34, 11, and 43 years. Please see Text S4 in Supporting Information S1 for the details about sensitivity of stress results. Diercks et al. (2023) examined the influence of source parameters of historical earthquakes on the simulated Coulomb stress change in western Turkey, yielding similar findings, and underscored the significance of better constraining the source parameters of historical earthquakes.

The impact of varying fault slip models of the 2023 earthquake doublets is also tested by using different dislocation models provided by USGS, Barbot et al., 2023, Jia et al. (2023), and Ren et al. (2024) (Text S5 in Supporting Information S1). We found that the maximum positive ΔCFS of the S2 rupture varied between 86 and 923 kPa caused by the S1 of the 2023 Mw 7.8 earthquake (Figure S26 in Supporting Information S1). The positive ΔCFS on the 2023 Mw 7.6 earthquake epicenter varied between 8 and 305 kPa caused by the 2023 Mw 7.8

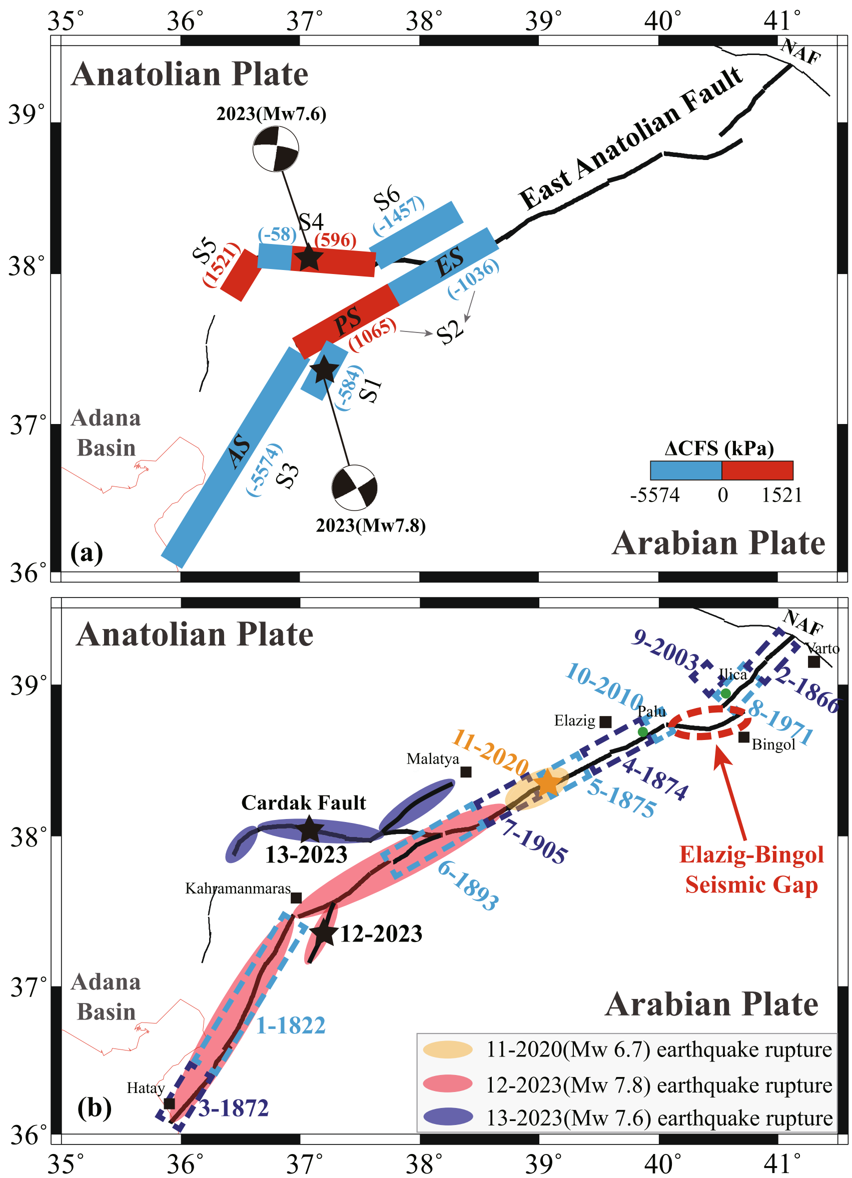

Figure 6. Schematic illustration of earthquake stress change distribution and rupture zones in the EAF region between 1822 and 2023. (a) The stress changes on the S1-S6 ruptures prior to their respective ruptures during the 2023 earthquake doublet. The segments on the EAF, including Amanos, Pazarcik, and Erkenek segments, are abbreviated as AS, PS, and ES, respectively. The red and blue rectangles represent areas of stress increase and decrease, respectively, with the maximum and minimum values of ΔCFS indicated beside the rectangles. NAF: North Anatolian Fault. (b) The earthquake rupture zones on the EAF between 1822 and 2019 (Ambraseys, 1989; Ambraseys & Jackson, 1998; Duman & Emre, 2013; Nalbant et al., 2002; Sunbul, 2019; Tan et al., 2008) are shown as blue dashed line rectangles, while the red dashed line ellipse marks the Elazig-Bingol seismic gap in the EAF (See Table S1 in Supporting Information S1 for the details of the earthquake parameters). The red, blue, and yellow elliptical zones represent the rupture areas of the 2023 Mw 7.8, 2023 Mw 7.6, and 2020 Mw 6.7 earthquakes, respectively (Chen et al., 2022; USGS Earthquake Hazards Program, 2017). The black and yellow stars mark the epicenters of the 2023 earthquake doublet and the 2020 earthquake, respectively.

earthquake (Figure S27 in Supporting Information S1). This indicates that the coseismic stress change on the S2 segment is highly dependent on the details of the slip distribution on the S1 segment.

It is important to note that we observed significant differences in the stress patterns and a change in the sign of stress on the S2 segment across four scenarios (Cases L1-1893, L2-1893, L1-1905, and L2-1905 in Supporting Information S1), depending on the locations of the 1893 M7.1 (No. 6) and 1905 M6.8 (No. 7) earthquakes (Figures S10c and S10e in Supporting Information S1). Positive stress appears in part of the Erkenek segment of the S2 as a result of these models. These findings are reasonable, as the rupture zones of the 1893 and 1905 earthquakes overlap within the Erkenek segment (Figure 6b). Positive static stress changes can reach several hundred to one thousand kPa around the fault edges of the 1893 M7.1 and 1905 M6.8 earthquakes, consistent with previous findings (Belardinelli et al., 1999; Liu et al., 2018; Oglesby et al., 2003).

Source or receiver orientation can affect stress patterns and potentially change the stress sign in the medium to far field. Our results indicate that the S1, S3, and S4 segments are situated near the positive and negative lobes of stress change induced by the 1905 M6.8 (No. 7) and 1939 M7.9 (No. 14) earthquakes (Figures S6g, S6k, S11k, and S13g in Supporting Information S1). Varying the orientation of the source or receiver fault might alter the stress sign in these cases. However, these events were not included in the sensitivity analysis because they do not produce significant stress changes when using nominal source parameters based on our results (Figures S6g, S6k, S11k, and S13g in Supporting Information S1). This result could vary slightly with different source mechanisms or receiver fault orientations.

The rheology of the Anatolian Plate's lithosphere is still under debate (Hearn & Bürgmann, 2005; Hearn et al., 2009; Sunbul, 2019; Sunbul et al., 2016). We assessed the effects on the stress results due to the viscosity of the ductile lower crust and lithospheric mantle. Our findings indicate that variations in viscosity have a significant impact on the stress results. For example, increasing the viscosity in the lower crust by a factor of 10 changed the ΔCFS from −154 kPa to −263 kPa at the 2023 Mw 7.8 earthquake epicenter. Similarly, increasing the viscosity in the lithospheric mantle by 10 and 100 times changed the ΔCFS after 2022 from −154 kPa to −215 kPa and −247 kPa, respectively, at the 2023 Mw 7.8 earthquake epicenter. Future research should focus on determining the rheological structure of the Anatolian Plate.

5. Conclusions

To better understand the earthquake interaction process and its impact on the seismic activities in EAF, we conducted simulations of the stress evolution before, during, and after 2023 induced by 21 earthquakes, including the six cascading sub-events of the 2023 earthquake doublet, during the past two centuries. We investigated the role of static stress change on the rupture initiation, propagation, and termination of the 2023 earthquake doublet, and analyzed the seismic hazards in the EAF and DSF seismic gaps. We reached the following conclusions.

1. The 2023 Mw 7.8 earthquake was delayed due to the stress shadow on the first sub-event (S1) on the Narli fault caused by 19 earthquakes between 1822 and 2022. The S1 triggered the already stressed Pazarcik segment of the second sub-event, resulting in its northeastward rupture propagating along the main branch of EAF. However, this northeastward rupture was terminated by the stress shadow created by the 2020 Mw 6.7 Elazig earthquake.
2. The 2023 Mw 7.6 earthquake was promoted due to stress increase on the fourth sub-event (S4) of the Mw 7.6 earthquake, caused by 19 historical earthquakes between 1822 and 2022. The Mw 7.8 earthquake provided the final kick to the already stressed S4 and advanced it for approximately 75 years due to the loading stress.
3. We revealed the process of how the stress changes induced by preceding sub-events can influence the occurrence and behavior of subsequent sub-events with the example of the 2023 Turkey-Syria earthquake doublet. The stress change induced by preceding sub-events, reaching several hundred to thousand kPa, is large enough to promote the subsequent sub-events during the earthquake doublet. It provided valuable insights for exploring earthquake preparation, rupture initiation, propagation, migration, and termination in structurally complex fault systems globally.
4. Special attention should be paid to the raised hazards due to the promoted stress in regions between Palu and Ilica cities in the Elazig-Bingol seismic gap of the EAF and the northern section of the DSF by historical earthquakes. This is important in the development of effective strategies for disaster prevention and relief in the populated regions in southeastern Turkey, northern Syria, and Lebanon.

Data Availability Statement

The data files used in this paper are available at (Liu, 2024).

Acknowledgments
Jianling Cao was supported by the National Natural Science Foundation of China (41974111). Chang Liu was supported by the National Natural Science Foundation of China (41974102). Guangliang Yang was supported by the National Natural Science Foundation of China (42174104, U1939204) and Hubei provincial Natural Science Foundation of China (2022CFB350). Hui Wang was supported by the National Natural Science Foundation of China (42274131). Luca Dal Zilio was supported by the EU project "A Digital Twin for Geophysical Extremes" (DT-GEO) (101058129) and the European Research Council (ERC) Synergy Grant "Fault Activation and Earthquake Rupture" (FEAR) (856559). Yaolin Shi was supported by the National Natural Science Foundation of China (U1839207). Oğuz Hakan Göğüş acknowledges financial support from ITU BAP unit project no: MUA-2019-42239 and ANATEC (ILP/International Lithosphere Program). We would like to thank Rachel Abercrombie (the editor), the associate editor, and two anonymous reviewers for their suggestions. We are grateful for Martin Mai, Roland Burgmann, Oliver Heidbach, Joe Aslin, and Tom Parsons for their suggestions. We would like to thank Ömer Budor, Tianhaozhe Sun, and Ebru Şengül Uluocak for helpful discussion.

References

Aktug, B., Ozener, H., Dogru, A., Sabuncu, A., Turgut, B., Halicioglu, K., et al. (2016). Slip rates and seismic potential on the East Anatolian Fault System using an improved GPS velocity field. *Journal of Geodynamics*, *94–95*, 1–12. https://doi.org/10.1016/j.jog.2016.01.001

Ambraseys, N. N. (1989). Temporary seismic quiescence: SE Turkey. *Geophysical Journal International*, *96*(2), 311–331. https://doi.org/10.1111/j.1365-246x.1989.tb04453.x

Ambraseys, N. N., & Jackson, J. A. (1998). Faulting associated with historical and recent earthquakes in the Eastern Mediterranean region. *Geophysical Journal International*, *133*(2), 390–406. https://doi.org/10.1046/j.1365-246x.1998.00508.x

Antonioli, A., Cocco, M., Das, S., & Henry, C. (2002). Dynamic stress triggering during the great 25 March 1998 Antarctic Plate earthquake. *Bulletin of the Seismological Society of America*, *92*(3), 896–903. https://doi.org/10.1785/0120010164

Aochi, H., Fukuyama, E., & Matsu'ura, M. (2000). Selectivity of spontaneous rupture propagation on a branched fault. *Geophysical Research Letters*, *27*(22), 3635–3638. https://doi.org/10.1029/2000gl011560

Arpat, E., & Saroglu, F. (1972). The East Anatolian Fault system: Thoughts on its development. *Bulletin of the Mineral Research and Exploration Institute of Turkey*, *78*, 33–39.

Artemieva, I. M., & Shulgin, A. (2019). Geodynamics of Anatolia: Lithosphere thermal structure and thickness. *Tectonics*, *38*(12), 4465–4487. https://doi.org/10.1029/2019TC005594

Barbot, S., Luo, H., Wang, T., Hamiel, Y., Piatibratova, O., Muhammad, T., et al. (2023). Slip distribution of the February 6, 2023 Mw 7.8 and Mw 7.6, Kahramanmaraş, Turkey earthquake sequence in the East Anatolian Fault Zone. *Seismica*, *3*(2). https://doi.org/10.26443/seismica.v2i3.502

Barka, A. (1996). Slip distribution along the North Anatolian fault associated with the large earthquakes of the period 1939 to 1967. *Bulletin of the Seismological Society of America*, *86*(5), 1238–1254. https://doi.org/10.1785/bssa0860051238

Bayrak, E., Yılmaz, Ş., Softa, M., Türker, T., & Bayrak, Y. (2015). Earthquake hazard analysis for East Anatolian Fault Zone, Turkey. *Natural Hazards*, *76*(2), 1063–1077. https://doi.org/10.1007/s11069-014-1541-5

Belardinelli, M. E., Bizzarri, A., & Cocco, M. (2003). Earthquake triggering by static and dynamic stress changes. *Journal of Geophysical Research*, *108*(B3). https://doi.org/10.1029/2002JB001779

Belardinelli, M. E., Cocco, M., Coutant, O., & Cotton, F. (1999). Redistribution of dynamic stress during coseismic ruptures: Evidence for fault interaction and earthquake triggering. *Journal of Geophysical Research*, *104*(B7), 14925–14945. https://doi.org/10.1029/1999jb900094

Biryol, C. B., Beck, S. L., Zandt, G., & Özacar, A. A. (2011). Segmented African lithosphere beneath the Anatolian region inferred from teleseismic P-wave tomography. *Geophysical Journal International*, *184*(3), 1037–1057. https://doi.org/10.1111/j.1365-246X.2010.04910.x

Cakir, Z., Doğan, U., Akoğlu, A. M., Ergintav, S., Özarpacı, S., Özdemir, A., et al. (2023). Arrest of the Mw 6.8 January 24, 2020 Elaziğ (Turkey) earthquake by shallow fault creep. *Earth and Planetary Science Letters*, *608*, 118085. https://doi.org/10.1016/j.epsl.2023.118085

Chen, J. Q., Liu, C., Zhang, H., & Shi, Y. L. (2022). Seismic activities and hazards of the seismic gaps in the Haiyuan fault in northeastern Tibet: Insights from numerical modelling earthquake interaction. *Earth and Space Science*, *9*(11), 1–14. https://doi.org/10.1029/2022ea002536

Chen, K., Wei, G., Milliner, C., Dal Zilio, L., Liang, C., & Avouac, J.-P. (2024). Super-shear ruptures steered by pre-stress heterogeneities during the 2023 Kahramanmaraş earthquake doublet. *Nature Communications*, *15*(1), 7004. https://doi.org/10.1038/s41467-024-51446-y

Chen, K., Zhang, Z., Liang, C., Xue, C., & Liu, P. (2020). Kinematics and dynamics of the 24 January 2020 M w 6.7 Elazig, Turkey earthquake. *Earth and Space Science*, *7*(11). https://doi.org/10.1029/2020EA001452

Confal, J., Faccenda, M., Eken, T., & Taymaz, T. (2018). Numerical simulation of 3-D mantle flow evolution in subduction zone environments in relation to seismic anisotropy beneath the eastern mediterranean region. *Earth and Planetary Science Letters*, *497*, 50–61. https://doi.org/10.1016/j.epsl.2018.06.005

Dal Zilio, L., & Ampuero, J.-P. (2023). Earthquake doublet in Turkey and Syria. *Communications Earth & Environment*, *4*(1), 71. https://doi.org/10.1038/s43247-023-00747-z

Delouis, B., van den Ende, M., & Ampuero, J.-P. (2023). *Kinematic rupture model of the February 6th 2023 Mw 7.8 Turkey earthquake from a large set of near-source strong motion records combined by GNSS offsets reveals intermittent supershear rupture*. Authorea. https://doi.org/10.22541/essoar.168286647.71550161/v1

Dewey, J. F., Hempton, M. R., Kidd, W. S. F., Saroglu, F., & Şengör, A. M. C. (1986). Shortening of continental lithosphere: The neotectonics of eastern Anatolia—A young collision zone. *Geological Society, London, Special Publications*, *19*(1), 1–36. https://doi.org/10.1144/gsl.sp.1986.019.01.01

Diercks, M.-L., Mildon, Z. K., Boulton, S. J., Hussain, E., Alçiçek, M. C., Yıldırım, C., & Aykut, T. (2023). Constraining historical earthquake sequences with Coulomb stress models: An example from western Türkiye. *Journal of Geophysical Research: Solid Earth*, *128*(11), e2023JB026627. https://doi.org/10.1029/2023JB026627

Ding, H., Zhou, Y., Ge, Z., Taymaz, T., Ghosh, A., Xu, H., et al. (2023). High-resolution seismicity imaging and early aftershock migration of the 2023 Kahramanmaraş (SE Türkiye) MW7. 9 & 7.8 earthquake doublet. *Earthquake Science*, *36*(6), 417–432. https://doi.org/10.1016/j.eqs.2023.06.002

Doğan, B., & Karakaş, A. (2013). Geometry of co-seismic surface ruptures and tectonic meaning of the 23 October 2011 Mw 7.1 Van earthquake (East Anatolian Region, Turkey). *Journal of Structural Geology*, *46*, 99–114. https://doi.org/10.1016/j.jsg.2012.10.001

Duan, B. (2010). Role of initial stress rotations in rupture dynamics and ground motion: A case study with implications for the Wenchuan earthquake. *Journal of Geophysical Research: Solid Earth*, *115*(B5). https://doi.org/10.1029/2009jb006750

Duan, B., & Oglesby, D. D. (2005). Multicycle dynamics of nonplanar strike-slip faults. *Journal of Geophysical Research: Solid Earth*, *1978–2012*(B3), 110. https://doi.org/10.1029/2004jb003298

Duan, B., & Oglesby, D. D. (2006). Heterogeneous fault stresses from previous earthquakes and the effect on dynamics of parallel strike-slip faults. *Journal of Geophysical Research: Solid Earth*, *111*(B5). https://doi.org/10.1029/2005jb004138

Duan, B., & Oglesby, D. D. (2007). Nonuniform prestress from prior earthquakes and the effect on dynamics of branched fault systems. *Journal of Geophysical Research*, *112*(B5). https://doi.org/10.1029/2006jb004443

Duman, T. Y., & Emre, Ö. (2013). The East Anatolian Fault: Geometry, segmentation and jog characteristics. *Geological Society, London, Special Publications*, *372*(1), 495–529. https://doi.org/10.1144/sp372.14

Eberhart-Phillips, D., Haeussler, P. J., Freymueller, J. T., Frankel, A. D., Rubin, C. M., Craw, P., et al. (2003). The 2002 Denali fault earthquake, Alaska: A large magnitude, slip-partitioned event. *Science*, *300*(5622), 1113–1118. https://doi.org/10.1126/science.1082703

Eken, T., Qashqai, M. T., Schiffer, C., Taymaz, T., & Saygin, T. (2021). New insights into crustal properties of Anatolia and its surroundings inferred from P-Coda autocorrelation inversions. *Journal of Geophysical Research: Solid Earth*, *126*(12). https://doi.org/10.1029/2021JB023184

Eyidogan, H., & Akinci, A. (1999). Site attenuation and source parameters on the North Anatolian Fault zone, eastern Turkey estimated from the aftershocks of 13 March 1992 Erzincan earthquake. *Journal of Seismology*, *3*(4), 363–373. https://doi.org/10.1023/A:1009833925675

Fan, W., Shearer, P. M., Ji, C., & Bassett, D. (2016). Multiple branching rupture of the 2009 Tonga-Samoa earthquake. *Journal of Geophysical Research: Solid Earth*, *121*(8), 5809–5827. https://doi.org/10.1002/2016jb012945

Fichtner, A., Trampert, J., Cupillard, P., Saygin, E., Taymaz, T., Capdeville, Y., & Villaseñor, A. (2013). Multi-scale full waveform inversion. *Geophysical Journal International*, *194*(1), 534–556. https://doi.org/10.1093/gji/ggt118

Freed, A. M. (2005). Earthquake triggering by static, dynamic, and postseismic stress transfer. *Annual Review of Earth and Planetary Sciences*, *33*(1), 335–367. https://doi.org/10.1146/annurev.earth.33.092203.122505

Freed, A. M., & Lin, J. (2001). Delayed triggering of the 1999 Hector Mine earthquake by viscoelastic stress transfer. *Nature*, *411*(6834), 180–183. https://doi.org/10.1038/35075548

Gabriel, A. A., Ulrich, T., Marchandon, M., Biemiller, J., & Rekoske, J. (2023). 3D dynamic rupture modeling of the 6 February 2023, Kahramanmaraş, Turkey M w 7.8 and 7.7 earthquake doublet using early observations. *The Seismic Record*, *3*(4), 342–356. https://doi.org/10.1785/0320230028

Gahalaut, V. K., Rajput, S., & Kundu, B. (2011). Low seismicity in the Bhutan Himalaya and the stress shadow of the 1897 Shillong Plateau earthquake. *Physics of the Earth and Planetary Interiors*, *186*(3), 97–102. https://doi.org/10.1016/j.pepi.2011.04.009

Goldberg, D. E., Taymaz, T., Reitman, N. G., Hatem, A. E., Yolsal-Çevikbilen, S., Barnhart, W. D., et al. (2023). Rapid characterization of the February 2023 Kahramanmaraş, Türkiye, earthquake sequence. *The Seismic Record*, *3*(2), 156–167. https://doi.org/10.1785/0320230009

Grosser, H., Baumbach, M., Berckhemer, H., Baier, B., Karahan, A., Schelle, H., et al. (1998). The Erzincan (Turkey) earthquake (Ms 6.8) of March 13, 1992 and its aftershock sequence. *Pure and Applied Geophysics*, *152*(3), 465–505. https://doi.org/10.1007/s000240050163

Güvercin, S. E., Karabulut, H., Konca, A. Ö., Doğan, U., & Ergintav, S. (2022). Active seismotectonics of the East Anatolian Fault. *Geophysical Journal International*, *230*(1), 50–69. https://doi.org/10.1093/gji/ggac045

Güvercin, S. E., Konca, A. Ö., Karabulut, H., Eskiköy, F., Hollingsworth, J., & Ergintav, S. (2023). Preliminary seismic and geodetic observations of the Mw7.8 and Mw7.6 earthquakes in eastern Turkey, EGU general assembly 2023, Vienna, Austria, 24–28 Apr 2023, EGU23-17619. https://doi.org/10.5194/egusphere-egu23-17619

Harris, R. A. (1998). Introduction to special section: Stress triggers, stress shadows, and implications for seismic hazard. *Journal of Geophysical Research: Solid Earth*, *103*(B10), 24347–24358. https://doi.org/10.1029/98jb01576

Harris, R. A., & Simpson, R. W. (1996). In the shadow of 1857 - The effect of the great Ft Tejon earthquake on subsequent earthquakes in southern California. *Geophysical Research Letters*, *23*(3), 229–232. https://doi.org/10.1029/96gl00015

He, L., Feng, G., Xu, W., Wang, Y., Xiong, Z., Gao, H., & Liu, X. (2023). Coseismic kinematics of the 2023 Kahramanmaras, Turkey earthquake sequence from InSAR and optical data. *Geophysical Research Letters*, *50*(17), e2023GL104693. https://doi.org/10.1029/2023GL104693

Hearn, E. H., & Bürgmann, R. (2005). The effect of elastic layering on inversions of GPS data for coseismic slip and resulting stress changes: Strike-slip earthquakes. *Bulletin of the Seismological Society of America*, *95*(5), 1637–1653. https://doi.org/10.1785/0120040158

Hearn, E. H., McClusky, S., Ergintav, S., & Reilinger, R. E. (2009). Izmit earthquake postseismic deformation and dynamics of the North Anatolian Fault zone. *Journal of Geophysical Research*, *114*(B8), B08405. https://doi.org/10.1029/2008JB006026

Hempton, M. R., Dewey, J. F., & Saroglu, F. (1981). *The East Anatolian transform fault: Along strike variations in geometry and behavior (abstract)*. EOS. 62393.

Hikima, K., & Koketsu, K. (2005). Rupture processes of the 2004 Chuetsu (mid-Niigata prefecture) earthquake, Japan: A series of events in a complex fault system: The 2004 Chuetsu, Japan, earthquake. *Geophysical Research Letters*, *32*(18). https://doi.org/10.1029/2005gl023588

Hreinsdóttir, S., Freymueller, J. T., Fletcher, H. J., Larsen, C. F., & Bürgmann, R. (2003). Coseismic slip distribution of the 2002 Mw7. 9 Denali fault earthquake, Alaska, determined from GPS measurements. *Geophysical Research Letters*, *30*(13), 1670. https://doi.org/10.1029/GL017447

Irmak, T. S., Dogan, B., & Karakas, A. (2012). Source mechanism of the 23 October 2011 Van (Turkey) earthquake (Mw ¼ 7.1) and aftershocks with its tectonic implications. *Earth Planets and Space*, *64*, 1e13.

Jackson, J. A., & McKenzie, D. (1984). Active tectonics of the Alpine-Himalayan belt between western Turkey and Pakistan. *Geophysical Journal of the Royal Astronomical Society*, *77*(1), 185–264. https://doi.org/10.1111/j.1365-246x.1984.tb01931.x

Jia, Z., Jin, Z., Marchandon, M., Ulrich, T., Gabriel, A. A., Fan, W., et al. (2023). The complex dynamics of the 2023 Kahramanmaraş, Turkey, M w 7.8-7.7 earthquake doublet. *Science*, *381*(6661), 985–990. https://doi.org/10.1126/science.adi0685

Kame, N., Rice, J. R., & Dmowska, R. (2003). Effects of prestress state and rupture velocity on dynamic fault branching. *Journal of Geophysical Research*, *108*(B5), 2265. https://doi.org/10.1029/2002JB002189

King, G. C. P., Stein, R. S., & Jian, L. (1994). Static stress changes and the triggering of earthquakes. *Bulletin of the Seismological Society of America*, *84*(3), 935–953.

Koç, A., & Kaymakcı, N. (2013). Kinematics of Sürgü fault zone (Malatya, Turkey): A remote sensing study. *Journal of Geodynamics*, *65*, 292–307. https://doi.org/10.1016/j.jog.2012.08.001

Kounoudis, R., Bastow, I. D., Ogden, C. S., Goes, S., Jenkins, J., Grant, B., & Braham, C. (2020). Seismic tomographic imaging of the eastern mediterranean mantle: Implications for terminal-stage subduction, the uplift of Anatolia, and the development of the North Anatolian Fault. *Geochemistry, Geophysics, Geosystems*, *21*(7). https://doi.org/10.1029/2020GC009009

Lasserre, C., Peltzer, G., Crampé, F., Klinger, Y., van Der Woerd, J., & Tapponnier, P. (2005). Coseismic deformation of the 2001 Mw = 7.8 Kokoxili earthquake in Tibet, measured by synthetic aperture radar interferometry. *Journal of Geophysical Research: Solid Earth*, *110*(B12). https://doi.org/10.1029/2004jb003500

Li, S., Wang, X., Tao, T., Zhu, Y., Qu, X., Li, Z., et al. (2023). Source model of the 2023 Turkey earthquake sequence Imagedby Sentinel-1 and GPS measurements: Implications for heterogeneous fault behavior along the East Anatolian Fault zone. *Remote Sensing*, *15*(10), 2618. https://doi.org/10.3390/rs15102618

Liu, C. (2024). Earthquake data in the East Anatolian Fault (version 2) [Dataset]. *Zenodo*. https://doi.org/10.5281/zenodo.13230079

Liu, C., Dong, P., & Shi, Y. (2017a). Stress change from the 2015 Mw 7.8 Gorkha earthquake and increased hazard in the southern Tibetan Plateau. *Physics of the Earth and Planetary Interiors*, *267*, 1–8. https://doi.org/10.1016/j.pepi.2017.04.002

Liu, C., Dong, P., Zhu, B., & Shi, Y. (2018). Stress shadow on the southwest portion of the Longmen Shan fault impacted the 2008 Wenchuan earthquake rupture. *Journal of Geophysical Research: Solid Earth*, *123*(11), 9963–9981. https://doi.org/10.1029/2018jb015633

Liu, C., Dong, P. Y., & Shi, Y. L. (2017b). Recurrence interval of the 2008 Mw 7.9 Wenchuan earthquake inferred from geodynamic modelling stress buildup and release. *Journal of Geodynamics*, *110*, 1–11. https://doi.org/10.1016/j.jog.2017.07.007

Liu, C., Lay, T., Wang, R., Taymaz, T., Xie, Z., Xiong, X., et al. (2023). Complex multi-fault rupture and triggering during the 2023 earthquake doublet in southeastern Türkiye. *Nature Communications*, *14*(1), 5564. https://doi.org/10.1038/s41467-023-41404-5

Liu, C., & Shi, Y. (2021). Space-time stress variations on the Palu-Koro fault impacting the 2018 Mw 7.5 Palu earthquake and its seismic hazards. *Geochemistry, Geophysics, Geosystems*, *22*(5), e2020GC009552. https://doi.org/10.1029/2020GC009552

Liu, C., & Shi, Y. L. (2022). The role of fault interaction on earthquake migration in central Sulawesi, Indonesia. *Tectonophysics*, *839*(20), 1–14.

Liu, C., Zhang, H., Chen, J., & Shi, Y. (2022). Stress evolution before and after the 2021 Mw 7.3 Maduo earthquake in northeastern Tibet and its influence on seismic hazards. *Earth and Space Science*, *9*(6), e2022EA002325. https://doi.org/10.1029/2022EA002325

Liu, C., Zhu, B., & Shi, Y. (2020). Do the two seismic gaps in the southwestern section of the Longmen Shan fault present the same seismic hazard? *Journal of Geophysical Research: Solid Earth*, *125*(3), e2019JB018160. https://doi.org/10.1029/2019JB018160

Liu, C., Zhu, B., Yang, X., & Shi, Y. (2016). Geodynamic background of the 2008 Wenchuan earthquake based on 3D visco-elastic numerical modelling. *Physics of the Earth and Planetary Interiors*, *252*, 23–36. https://doi.org/10.1016/j.pepi.2016.01.003

Liu, C., Zhu, B. J., & Shi, Y. L. (2016). Lithospheric rheology and Moho upheaval control the generation mechanism of the intraplate earthquakes in the North China Basin. *Journal of Asian Earth Sciences*, *121*, 153–164. https://doi.org/10.1016/j.jseaes.2016.03.008

Lozos, J. C. (2016). A case for historic joint rupture of the San Andreas and San Jacinto faults. *Science Advances*, *2*(3), e1500621. https://doi.org/10.1126/sciadv.1500621

Lyberis, N., Yürür, T., Chorowicz, J., Kasapoglu, E., & Gundogdu, N. (1982). The East Anatolian Fault: An oblique collisional belt. *Tectonophysics*, *204*(1–2), 1–15. https://doi.org/10.1016/0040-1951(92)90265-8

Mahatsente, R., Önal, G., & Çemen, İ. (2018). Lithospheric structure and the isostatic state of Eastern Anatolia: Insight from gravity data modelling. *Liyhosphere*, *10*(2), 279–290. https://doi.org/10.1130/l685.1

Mai, P. M., Aspiotis, T., Aquib, T. A., Cano, E. V., Castro-Cruz, D., Espindola-Carmona, A., et al. (2023). The destructive earthquake doublet of 6 February 2023 in south-central Türkiye and northwestern Syria: Initial observations and analyses. *The Seismic Record*, *3*(2), 105–115. https://doi.org/10.1785/0320230007

Mallman, E. P., & Parsons, T. (2008). A global search for stress shadows. *Journal of Geophysical Research*, *113*(B12). https://doi.org/10.1029/2007JB005336

Manga, M., Beresnev, I., Brodsky, E. E., Elkhoury, J. E., Elsworth, D., Ingebritsen, S. E., et al. (2012). Changes in permeability caused by transient stresses: Field observations, experiments, and mechanisms. *Reviews of Geophysics*, *50*(2). https://doi.org/10.1029/2011rg000382

Medved, I., Polat, G., & Koulakov, I. (2021). Crustal structure of the eastern Anatolia region (Turkey) based on seismic tomography. *Geosciences*, *11*(2), 91. https://doi.org/10.3390/geosciences11020091

Meghraoui, M., Gomez, F., Sbeinati, R., Van Der Woerd, J., Mouty, M., Darkal, A. N., et al. (2003). Evidence for 830 years of seismic quiescence from palaeoseismology, archaeoseismology and historical seismicity along the Dead Sea fault in Syria. *Earth and Planetary Science Letters*, *210*(1–2), 35–52. https://doi.org/10.1016/s0012-821x(03)00144-4

Melgar, D., Taymaz, T., Ganas, A., Crowell, B., Öcalan, T., Kahraman, M., et al. (2023). Sub- and super-shear ruptures during the 2023 Mw 7.8 and Mw 7.6 earthquake doublet in SE Türkiye. *Seismica*, *2*(3). https://doi.org/10.26443/seismica.v2i3.387

Milkereit, C., Grosser, H., Wang, R. J., Wetzel, H. U., Woith, H., Karakisa, S., et al. (2004). Implications of the 2003 Bingol earthquake for the interaction between the north and east Anatolian faults. *Bulletin of the Seismological Society of America*, *94*(6), 2400–2406. https://doi.org/10.1785/0120030194

Mohammadi, H. (2022). Possible influence of static and viscoelastic stress perturbations in Musgrave block (Central Australia) earthquake sequence. *Physics of the Earth and Planetary Interiors*, *322*, 106830. https://doi.org/10.1016/j.pepi.2021.106830

Muehlberger, W. R., & Gordon, M. B. (1987). Observations on the complexity of the east anatolian fault, Turkey. *Journal of Structural Geology*, *9*(7), 899–903. https://doi.org/10.1016/0191-8141(87)90091-5

Nalbant, S. S., McCloskey, J., Steacy, S., & Barka, A. A. (2002). Stress accumulation and increased seismic risk in eastern Turkey. *Earth and Planetary Science Letters*, *195*(3–4), 291–298. https://doi.org/10.1016/s0012-821x(01)00592-1

Nissen, E., Elliott, J. R., Sloan, R. A., Craig, T. J., Funning, G. J., Hutko, A., et al. (2016). Limitations of rupture forecasting exposed by instantaneously triggered earthquake doublet. *Nature Geoscience*, *9*(4), 330–336. https://doi.org/10.1038/ngeo2653

Ogden, C. S., & Bastow, I. D. (2022). The crustal structure of the Anatolian Plate from receiver functions and implications for the uplift of the central and eastern Anatolian plateaus. *Geophysical Journal International*, *229*(2), 1041–1062. https://doi.org/10.1093/gji/ggab513

Oglesby, D. D., Day, S. M., & O'Connell, D. R. (2003). Dynamic and static interaction of two thrust faults: A case study with general implications. *Journal of Geophysical Research Solid Earth*, *108*(B10). https://doi.org/10.1029/2002jb002228

Okuwaki, R., Yuji, Y., Taymaz, T., & Hicks, S. (2023). Multi-scale rupture growth with alternating directions in a complex fault network during the 2023 south-eastern Türkiye and Syria earthquake doublet (preprint). https://doi.org/10.31223/X5RD4W

Ozacar, A. A., Zandt, G., Gilbert, H., & Beck, S. L. (2010). Seismic images of crustal variations beneath the East Anatolian Plateau (Turkey) from teleseismic receiver functions. *Geological Society, London, Special Publications*, *340*(1), 485–496. https://doi.org/10.1144/sp340.21

Payne, R. M., & Duan, B. (2015). Influence of initial stress and rupture initiation parameters on forbidden zone rupture propagation. *Geophysical Journal International*, *201*(1), 70–77. https://doi.org/10.1093/gji/ggv004

Pinar, A., Honkura, Y., & Kikuchi, M. (1994). Rupture process of the 1992 Erzincan earthquake and its implication for seismotectonic in eastern Turkey. *Geophysical Research Letters*, *21*(18), 1971–1974. https://doi.org/10.1029/94gl01712

Pollitz, F. F., & Sacks, S. I. (2002). Stress triggering of the 1999 Hector Mine earthquake by transient deformation following the 1992 Landers earthquake. *Bulletin of the Seismological Society of America*, *92*, 1487–1496.

Portner, D. E., Delph, J. R., Biryol, C. B., Beck, S. L., Zandt, G., Özacar, A. A., et al. (2018). Subduction termination through progressive slab deformation across Eastern Mediterranean subduction zones from updated P-wave tomography beneath Anatolia. *Geosphere*, *14*(3), 907–925. https://doi.org/10.1130/ges01617.1

Ramos, M. D., Neo, J. C., Thakur, P., Huang, Y., & Wei, S. (2020). Stress changes on the Garlock fault during and after the 2019 Ridgecrest earthquake sequence. *Bulletin of the Seismological Society of America*, *110*(4), 1752–1764. https://doi.org/10.1785/0120200027

Reasenberg, P. A., & Simpson, R. W. (1992). Response of regional seismicity to the static stress change produced by the Loma Prieta earthquake. *Science*, *255*(5052), 1687–1690. https://doi.org/10.1126/science.255.5052.1687

Reilinger, R., McClusky, S., Vernant, P., Lawrence, S., Ergintav, S., Cakmak, R., et al. (2006). GPS constraints on continental deformation in the Africa-Arabia-Eurasia continental collision zone and implications for the dynamics of plate interactions: Eastern mediterranean active tectonics. *Journal of Geophysical Research*, *111*(B5). https://doi.org/10.1029/2005JB004051

Ren, C., Wang, Z., Taymaz, T., Hu, N., Luo, H., Zhao, Z., et al. (2024). Supershear triggering and cascading fault ruptures of the 2023 Kahramanmaraş, Türkiye, earthquake doublet. *Science*, *383*(6680), 305–311. https://doi.org/10.1126/science.adi1519

Robertson, A. H. F. (2000). In E. Bozkurt, J. A. Winchester, & J. D. A. Piper (Eds.), *Mesozoic-tertiary tectonic sedimentary evolution of a south Tethyan oceanic basin and its margins in southern Turkey, in tectonics and magmatism in Turkey and the surrounding area 173* (pp. 97–138). Geological Society Special Publication.

Rojstaczer, S., Wolf, S., & Michel, R. (1995). Permeability enhancement in the shallow crust as a cause of earthquake-induced hydrological changes. *Nature*, *373*(6511), 237–239. https://doi.org/10.1038/373237a0

Shaddox, H. R., Schwartz, S. Y., & Bartlow, N. M. (2021). Afterslip and spontaneous aseismic slip on the Anza segment of the San Jacinto Fault zone, southern California. *Journal of Geophysical Research: Solid Earth*, *126*(6), e2020JB020460. https://doi.org/10.1029/2020jb020460

10.1029/2024JB029213

Shi, Y. L., & Cao, J. L. (2010). Some aspects of static stress change calculation—Case study on the Wenchuan earthquake. *Chinese Journal of Geophysics*, *53*(1), 64–73.

Simpson, R. W., Schulz, S. S., Dietz, L. D., & Burford, R. O. (1988). The response of creeping parts of the San Andreas fault to earthquakes on nearby faults: Two examples. *Pure and Applied Geophysics*, *126*(2), 665–685. https://doi.org/10.1007/bf00879014

Stein, R. S. (1999). The role of stress transfer in earthquake occurrence. *Nature*, *402*(6762), 605–609. https://doi.org/10.1038/45144

Sunbul, F. (2019). Time-dependent stress increase along the major faults in eastern Turkey. *Journal of Geodynamics*, *126*, 23–31. https://doi.org/10.1016/j.jog.2019.03.001

Sunbul, F., Nalbant, S. S., Simão, N. M., & Steacy, S. (2016). Investigating viscoelastic postseismic deformation due to large earthquakes in East Anatolia, Turkey. *Journal of Geodynamics*, *94*, 50–58. https://doi.org/10.1016/j.jog.2016.01.002

Tan, O., Pabuçcu, Z., Tapırdamaz, M. C., İnan, S., Ergintav, S., Eyidoğan, H., et al. (2011). Aftershock study and seismotectonic implications of the 8 March 2010 Kovancılar (Elazığ, Turkey) earthquake (MW = 6.1). *Geophysical Research Letters*, *38*(11). https://doi.org/10.1029/2011GL047702

Tan, O., Tapirdamaz, M. C., & Yörük, A. (2008). The earthquake catalogues for Turkey. *Turkish Journal of Earth Sciences*, *17*(2), 405–418.

Taufiqurrahman, T., Gabriel, A.-A., Li, D., Ulrich, T., Li, B., Carena, S., et al. (2023). Dynamics, interactions and delays of the 2019 Ridgecrest rupture sequence. *Nature*, *618*(7964), 1–8. https://doi.org/10.1038/s41586-023-05985-x

Taymaz, T., Ganas, A., Yolsal-Çevikbilen, S., Vera, F., Eken, T., Erman, C., et al. (2021). Source mechanism and rupture process of the 24 January 2020 Mw 6.7 Doğanyol–sivrice earthquake obtained from seismological waveform analysis and space geodetic observations on the East Anatolian Fault Zone (Turkey). *Tectonophysics*, *5*(804), 228745. https://doi.org/10.1016/j.tecto.2021.228745

Taymaz, T., Jackson, J., & McKenzie, D. (1991). Active tectonics of the north and central Aegean Sea. *Geophysical Journal International*, *106*(2), 433–490. https://doi.org/10.1111/j.1365-246x.1991.tb03906.x

Tesauro, M., Kaban, M. K., Petrunin, A. G., El Khrepy, S., & Al-Arifi, N. (2018). Strength and elastic thickness variations in the Arabian plate: A combination of temperature, composition and strain rates of the lithosphere. *Tectonophysics*, *746*, 398–411. https://doi.org/10.1016/j.tecto.2017.03.004

Toda, S., & Stein, R. S. (2024). The role of stress transfer in rupture nucleation and inhibition in the 2023 Kahramanmaraş, Türkiye, sequence, and a one-year earthquake Forecast. *Seismological Research Letters*, *95*(2A), 596–606. https://doi.org/10.1785/0220230252

Türkelli, N., Sandvol, E., Zor, E., Gok, R., Bekler, T., Al-Lazki, A., et al. (2003). Seismogenic zones in eastern Turkey. *Geophysical Research Letters*, *30*(24), 8039. https://doi.org/10.1029/2003GL018023

Ulrich, T., Gabriel, A.-A., Ampuero, J.-P., & Xu, W. (2019). Dynamic viability of the 2016 Mw 7.8 Kaikōura earthquake cascade on weak crustal faults. *Nature Communications*, *10*(1), 1213. https://doi.org/10.1038/s41467-019-09125-w

U.S. Geological Survey (USGS) Earthquake Hazards Program. (2017). *Advanced National Seismic System (ANSS) comprehensive catalog of earthquake events and products*. U.S. Geol. Surv. Data Release. https://doi.org/10.5066/F7MS3QZH

Utkucu, M. (2013). 2011 Van, eastern Anatolia, earthquake (MW7.1) and seismotectonics of lake van area. *Journal of Seismology*, *17*(2), 783–805. https://doi.org/10.1007/s10950-012-9354-z

Vanacore, E. A., Taymaz, T., & Saygin, E. (2013). Moho structure of the Anatolian Plate from receiver function analysis. *Geophysical Journal International*, *193*(1), 329–337. https://doi.org/10.1093/gji/ggs107

Wang, H., Huang, Z., Eken, E., Keleş, D., Kaya-Eken, T., Confal, J. M., et al. (2020). Isotropic and Anisotropic P-wave velocity structures of the crust and uppermost mantle beneath Turkey. *Journal of Geophysical Research: Solid Earth*, *125*(12), e2020JB019566. https://doi.org/10.1029/2020JB019566

Wang, R., Lorenzo Martín, F., & Roth, F. (2003). Computation of deformation induced by earthquakes in a multi-layered elastic crust - FORTRAN programs EDGRN/EDCMP. *Computers & Geosciences*, *29*(2), 195–207.

Wang, R., Lorenzo-Martín, F., & Roth, F. (2006). PSGRN/PSCMP-a new code for calculating co- and post-seismic deformation, geoid and gravity changes based on the viscoelastic-gravitational dislocation theory. *Computers & Geosciences*, *32*(4), 527–541. https://doi.org/10.1016/j.cageo.2005.08.006

Wang, Z., Zhang, W., Taymaz, T., He, Z., Xu, T., & Zhang, Z. (2023). Dynamic rupture process of the 2023 Mw 7.8 Kahramanmaraş earthquake (SE Türkiye): Variable rupture speed and implications for seismic hazard. *Geophysical Research Letters*, *50*(15), e2023GL104787. https://doi.org/10.1029/2023gl104787

Wells, D. L., & Coppersmith, K. J. (1994). New empirical relationships among magnitude, rupture length, rupture width, rupture area, and surface displacement. *Bulletin of the Seismological Society of America*, *84*(4), 974–1002. https://doi.org/10.1785/BSSA0840040974

Wen, Y. Y., Oglesby, D. D., Duan, B., & Ma, K. F. (2012). Dynamic rupture simulation of the 2008 M W 7.9 Wenchuan earthquake with heterogeneous initial stress. *Bulletin of the Seismological Society of America*, *102*(4), 1892–1898. https://doi.org/10.1785/0120110153

Whitney, D. L., Delph, J. R., Thomson, S. N., Beck, S. L., Brocard, G. Y., Cosca, M. A., et al. (2023). Breaking plates: Creation of the East Anatolian fault, the Anatolian plate, and a tectonic escape system. *Geology*, *51*(7), 673–677. https://doi.org/10.1130/g51211.1

Xu, L., Mohanna, S., Meng, L., Ji, C., Ampuero, J.-P., Yunjun, Z., et al. (2023). The 2023 Mw 7.8 Kahramanmaraş, Turkey earthquake: A multi-segment rupture in a millennium supercycle. *Research Square*. https://doi.org/10.21203/rs.3.rs-2747911/v1

Yamashita, T., & Umeda, Y. (1994). Earthquake rupture complexity due to dynamic nucleation and interaction of subsidiary faults. *Pure and Applied Geophysics*, *143*(1–3), 89–116. https://doi.org/10.1007/bf00874325

Yue, H., Lay, T., & Koper, K. D. (2012). En échelon and orthogonal fault ruptures of the 11 April 2012 great intraplate earthquakes. *Nature*, *490*(7419), 245–249. https://doi.org/10.1038/nature11492

Zahradník, J., Turhan, F., Sokos, E., & Gallovič, F. (2023). Asperity-like (segmented) structure of the 6 February 2023 Turkish earthquakes (preprint). *Geophysics and Seismology*. https://doi.org/10.31223/X5T666

Zeng, Y. (2001). Viscoelastic stress-triggering of the 1999 Hector mine earthquake by the 1992 Landers earthquake. *Geophysical Research Letters*, *28*(15), 3007–3010. https://doi.org/10.1029/2000gl012806

Zhang, Y., Tang, X., Liu, D., Taymaz, T., Eken, T., Guo, R., et al. (2023). Geometric controls on cascading rupture of the 2023 Kahramanmaraş earthquake doublet. *Nature Geoscience*, *16*(11), 1054–1060. https://doi.org/10.1038/s41561-023-01283-3

Zhu, H. (2018). High Vp/Vs ratio in the crust and uppermost mantle beneath volcanoes in the Central and Eastern Anatolia. *Geophysical Journal International*, *214*(3), 2151–2163. https://doi.org/10.1093/gji/ggy253